Journal of Molecular Liquids 414 (2024) 125999

Contents lists available at ScienceDirect

Journal of Molecular Liquids

journal homepage: www.elsevier.com/locate/molliq

Exploring the interaction of Cu-modified $B_{12}N_{12}$ nanocages for Favipiravir drug delivery using density functional theory study

Mohammad A. Matin [a,*], Joyanta K. Saha [b], Tapas Debnath [c], Joonkyung Jang [d]

[a] Computing Research Laboratory, Centre for Advanced Research in Sciences (CARS), Dhaka University, Dhaka 1000, Bangladesh
[b] Department of Chemistry, Jagannath University, Dhaka 1100, Bangladesh
[c] Department of Theoretical and Computational Chemistry, Dhaka University, Dhaka 1000, Bangladesh
[d] Department of Nanoenergy Engineering, Pusan National University, Busan 46241, South Korea

ARTICLE INFO

Keywords:
Favipiravir
$CuB_{11}N_{12}$ nanocage
Drug delivery
Density Functional Theory

ABSTRACT

Drug delivery has become a pivotal strategy in medical research, aiming for precise delivery near cells while minimizing unwanted effects. In this study, we have used density functional theory (DFT) calculations at the B3LYP/6-311G(d,p) basis set to explore the potential of Cu-modified boron nitride ($B_{12}N_{12}$) nanocages as smart nanocarriers for delivering the Favipiravir (FAV) drug. This study examined the adsorption energy, electronic features, and thermodynamic properties (ΔG and ΔH) of FAV with $B_{12}N_{12}$ and Cu-modified $B_{12}N_{12}$ nanocages, revealing enhanced drug-delivery capacity with notable physisorption and negative adsorption energies. A comprehensive analysis confirmed FAV's interaction with Cu-modified $B_{12}N_{12}$ nanocages, involving frontier molecular orbitals, adsorption energy, fractional charge transfer, molecular electrostatic potential (MEP), non-covalent interaction (NCI), and natural bond orbital (NBO) assessments. The analyses of frontier molecular orbitals (FMO), partial density of states (PDOS), and natural bond orbital (NBO) indicate that nanocages act as charge acceptors, while the drug acts as a charge donor during the adsorption process. Among the various Cu-modified $B_{12}N_{12}$ nanocages studied, Cu-doped $CuB_{11}N_{12}$ emerged as the most promising candidate for transporting FAV, showcasing notably moderate recovery time (ranging from 29.01 ms to 7.25 s at 298.15 K). Remarkably, the $CuB_{11}N_{12}$ system exhibited exceptional electronic sensitivity (ΔE_{gap} = 65.38 %) to the FAV drug, surpassing other modified systems. Among the modified cases, the Cu-decorated Cu@b64 and Cu@b66 nanocages showed the most significant decrease in energy levels before and after FAV absorption, reducing from 3.28 eV and 3.33 eV to 1.54 eV and 1.59 eV, respectively. This elucidation may lay the foundation for developing effective drug-delivery systems using nanocages for targeted therapies. In conclusion, this study offers a comprehensive insight into the interaction mechanism between the FAV drug and $B_{12}N_{12}$, unveiling the potential of Cu-modified $B_{12}N_{12}$ nanocages as promising candidates for delivering the FAV drug.

1. Introduction

FAV has gained attention for its broad-spectrum inhibitory potential in the treatment of RNA viral infections such as COVID-19 [1–3]. Primarily developed by Shi et al. [4], its exact introduction in COVID-19 treatment remains unclear [5]. FAV, though a universal inhibitor, has notable harmful aspect such as teratogenicity, weight loss, vomiting, hyperuricemia, liver damage, and renal injury [6]. To minimize adverse fallouts and increase particularity, smart and effective drug delivery systems for FAV must be developed. This approach enhances efficacy and minimizes side effects, providing a chosen and safer treatment for patients.

Nanomaterials are essential in nanoscience and nanotechnology due to their unique optical, magnetic, and electrical properties [7]. Due to their potential applications in diverse fields, such as medicine, electronics, and the chemical industry, researchers have shown a significant interest in these features [8]. Due to their versatility, there is a strong demand for the development of advanced, cost-effective sensing materials that can detect and reduce the adverse effects of drugs like FAV [9]. Due to their high adsorption capacities, excellent sensing performance, fast detection potential, and cramped electronic configurations within clusters, they are the perfect choice [10–14].

The stability of boron nitride nanocages, particularly small fullerene-type structures such as ($B_{12}N_{12}$), makes them valuable for biosensing applications [13,15]. The sensing capabilities of these structures can be

* Corresponding author.
E-mail address: matin123@du.ac.bd (M.A. Matin).

https://doi.org/10.1016/j.molliq.2024.125999
Received 19 March 2024; Received in revised form 10 September 2024; Accepted 11 September 2024
Available online 20 September 2024
0167-7322/© 2024 Elsevier B.V. All rights are reserved, including those for text and data mining, AI training, and similar technologies.

Parameters used in formulas and abbreviations

Abbr.	Parameters
E_{coh}	Cohesive energy
P	Total Number of atoms
E	Energy
$E_{nanocgae}$	Energy of nanocage surface
E_g	Energy gap
E_{HOMO}	Energy of highest occupied molecular orbital
E_{LUMO}	Energy of lowest unoccupied molecular orbital
ΔE_γ	Electronic sensitivity value
$E_{g(nanocage\text{-}FAV)}$	Band gap of nanocage-FAV complex
$E_{g(nanocage)}$	Band gap of nanocage
E_{ads}	Adsorption energy
$E_{ads,CP}$	Basis set superposition error corrected adsorption energy
E_{int}	Interaction energy
E_{FAV}	Energy of FAV drug
Φ	Work function
$V_{el(+\infty)}$	vacuum electrostatic potential energy
E_F	Fermi energy level
j	Current density
A	Richardson constant
E_{gas}	Total energy of the complex in gas phase
E_{water}	Total energy of the complex in water media
QCT	Charge transfer
ω	Electrophilicity index
μ	Electronic chemical potential
S	Chemical softness
η	Chemical hardness
CPCM	Conductor-like polarizable continuum model
DOS	Density of States
NCI	non-covalent interactions
VMD	Visual molecular dynamics
RDG	Reduced density gradient
τ	Recovery Time
ν	Frequency
σ	Rate constant
$\Delta\Sigma$	Entropy
ΔH	Enthalpy
$\Delta\Gamma$	Gibbs free energy
T	Temperature
K	Boltzmann's constant
$\rho(r)$	Electron Density
S(r)	Reduced density gradient
E_{sol}	Solvation energy

enhanced by doping with transition metal atoms [16–18], an approach known to improve sensor performance, along with C-doping [19].

Jensen and Toftlundt showed that $B_{12}N_{12}$ nanostructures were structurally strong and identified six tetragonal and eight hexagonal rings in four potential nanostructures via HF and MP2 methods [20]. The stability of the $B_{12}N_{12}$ nanocage was confirmed through theoretical research conducted after the fundamental study [21–23]. Oku *et* al. [24] later experimentally synthesized the $B_{12}N_{12}$ nanocage via arc-melting, validating earlier theoretical findings [20,21,23]. Significant efforts have been made to synthesize fullerene-like boron nitride nanocages [25–27] and Zhu *et al.* [25] successfully produced $B_{12}N_{12}$ nanocages in large quantities using a homemade B–N–O precursor.

Multiple research groups have examined how size and doping affect nanomaterials, concentrating on drug-bearing performance and physicochemical properties to enhance device capacity. Kurban *et al.* investigated the size-dependent adsorption performance of ZnO nanoclusters for drug delivery operations [28]. The sensing, electronic, and optical properties of boron nitride nanostructures were investigated by Muz *et al.* who observed how these properties change with diameter and size [29,30]. Assessing the cytotoxicity of nanomaterials is pivotal for their suitability in biological applications. Recent investigations have found the cytotoxicity and biocompatibility of carbon and BN nanostructures to be promising [31–33]. Researchers have extensively used DFT computational techniques to study both boron nitrides and drugs like FAV [34]. Cao *et al.* examined the adsorption behavior of penicillamine on pure $B_{12}N_{12}$ using DFT methods and compared it with its behavior in solvents like water and chloroform [35]. The drug was shown to have chemisorbed onto the nanocages and had high reactivity and conductivity, as indicated by their results and supported by thermodynamic studies. The influence of B, Si, and Al-modified fullerene C60 on adsorption of 5-FU was studied by Hazrati and Hadipour, which provided insight into their adsorption capabilities [36]. Furthermore, there have been extensive theoretical and experimental studies that have examined how pharmaceutical drugs adsorb onto BN nanomaterials [37], highlighting their diverse potential applications. To explore drug delivery efficiency, research on 5-ALA with $B_{12}N_{12}$ and $B_{16}N_{16}$ nanoclusters provided valuable information into the potential of these nanocages for drug delivery [38]. The ability of Si-doped and undoped fullerene (C60) to sense the FAV drug molecule was investigated by Parlak *et al.* [39]. Recent studies by Rad *et al.* [40] examined the sensing capabilities of first-row transition metal-doped fullerenes (C20) for FAV, indicating that Fe, Cr, and Ni-doped fullerenes may serve as effective drug carriers for COVID-19 treatment. Guo *et al.* carried out extensive theoretical and experimental research on BN nanomaterials and their doped derivatives to assess their potential for melphalan adsorption and detection [41]. Moreover, several investigations in the literature have demonstrated that $B_{12}N_{12}$ and its derivatives possess the capability to adsorb a wide array of medications, comprising 5-Fluorouracil [42–44], Sulfasalazine [45], Naproxen [46], Serine [47], Fluoroquinolone [48], Metformin [49], Chlormethine [50], Amphetamine [51], Flucytosine [52], Emodin [53], Azacitidine [54], Mercaptopyridine [55], Curcumin [56,57], penicillamine [58], Favipiravir [59–62], Aloe-emodin [63], Thiazole [64], Cladribine [65], Alprazolam [66], Allopurinol [67], Hydroxyurea [68], 1,3,4-oxadiazole [69], Hydroxyurea [70,71], Gemifloxacin [72], Ciprofloxacin [73], isoniazid [74], 6-Thioguanine [75], Temozolomide [76], Procarbazine [77], ifosfamide [78,79], Dacarbazine [80], Sulfasalazine [81], Carmustine [82], and Nitrosourea [83,84]. The significant potential of nanocage clusters in biomedicine, which includes biosensing, bioimaging, and targeted delivery of biological and medicinal substances, is brought to the attention in these achievements.

Intermolecular interactions between the FAV drug and Cu-modified $B_{12}N_{12}$ nanocages are very important. These interactions determine the stability, orientation, and effectiveness of the drug delivery system. Strong forces like hydrogen bonding, van der Waals interactions (vdW), and electrostatic attractions help the FAV drug bind firmly to the nanocages. This secure attachment is crucial for transporting the drug to the target site. These interactions also affect adsorption and deformation energies, which show positive values indicating some distortion. Understanding and improving these interactions can make the drug delivery system more efficient and effective, leading to better treatment results.

Despite advancements, the adsorption of FAV onto $B_{12}N_{12}$ fullerenes modified with late transition metals like copper remains unexplored. Early transition metals bind tightly to these surfaces, making separation difficult. In contrast, late transition metals, like copper, exhibit more reasonable affinity for binding to these surfaces. A previous study has demonstrated the energetically stable nature of Cu-modified nanocages, such as doped ($CuB_{11}N_{12}$ and $B_{12}N_{11}Cu$), decorated (Cu@b64 and

Cu@b66), and encapsulated Cu@$B_{12}N_{12}$ [85]. These observations motivated the development of a system employing Cu-modification on $B_{12}N_{12}$ to effectively bind the FAV drug and aid in its removal from toxic environments.

The objective of this study is to identify materials that possess the most potent drug-carrying and sensing capabilities for the FAV drug, with a focus on both unmodified and Cu-modified boron nitride ($B_{12}N_{12}$) nanocages. The $B_{12}N_{12}$ nanosurface was systematically modified by incorporating Cu metal in doped, decorated, and encapsulated positions. DFT methods were used to analyze structural, physical, electronic, adsorption, and thermodynamic properties theoretically in order to identify a suitable drug-carrying agent for FAV. The results of this study may offer valuable insights for designing drug carriers and nanomaterial-based sensors for favipiravir.

2. Computational methodology

This study thoroughly examined the potential of the Cu-modified $B_{12}N_{12}$ nanocarrier to adsorb Favipiravir (FAV). In this research, we used GaussView 6 to design the drug molecule and Cu-modified $B_{12}N_{12}$ nanocages, and Gaussian16 program [86] to optimize their minimum energy structures. Density functional theory (DFT) calculations were conducted to examine the adsorption phenomenon and interaction probability between the FAV drug and Cu-modified $B_{12}N_{12}$. Researchers may utilize different approaches to examine the desired feature. However, Fig. S1 outlines a standard procedure for conducting DFT calculations. Optimization and energy calculations for various configurations of the drug and Cu-modified $B_{12}N_{12}$ were performed using the B3LYP functional and the 6-311G(d,p) basis set, due to their well-established accuracy and reliability in computational chemistry which extensively used for nanocluster investigations [87,88]. Vibrational frequencies were calculated for the optimized geometries to confirm they were true minima, as evidenced by the absence of imaginary frequencies. A scaling factor of 0.957 was applied to the vibrational frequencies. The structures studied were neutral (total charge of zero) and stabilized with a singlet multiplicity (M=2S+1, where S is the total spin) for the $CuB_{11}N_{12}$ and $B_{12}N_{11}Cu$ nanocages, while a doublet multiplicity was used for the Cu@b64, Cu@b66, and Cu@$B_{12}N_{12}$ nanocages.

To assess the structural stability of the nanocages, the cohesive energy (E_{coh}) was computed using Eq. (1); [53,89]

$$E_{coh} = \frac{1}{P}\left(E_{nanocage} - xE_B - yE_N - zE_{Cu}\right) \quad (1)$$

where, $E_{nanocage}$ represents the total energy of the nanocages(pure and Cu-modified); E_B, E_N, and E_{Cu} represent the energies of boron (B), nitrogen (N), and the doped metal (Cu), respectively. The quantities x, y, and z represent the number of boron, nitrogen, and doped metal atoms, respectively, while P denotes the total number of atoms in the system. Notably, z = 0 indicated pristine structure, while z = 1 represented Cu-modified structures, including $CuB_{11}N_{12}$ and $B_{12}N_{11}Cu$ (doped structures), Cu@b66 and Cu@b64 (decorated structures), and Cu@$B_{12}N_{12}$ (encapsulated structure). The E_g value is defined as Eq. (2);

$$E_g = E_{HOMO} - E_{LUMO} \quad (2)$$

The E_g value, which identifies the energy gap between the energy of highest occupied molecular orbital (E_{HOMO}) and energy of the lowest unoccupied molecular orbital (E_{LUMO}), has major significance in understanding electronics and reactivity.

For the evaluation of the electronic sensitivity value (ΔE_g) regarding the interaction between FAV and either pure $B_{12}N_{12}$ or Cu-modified $B_{12}N_{12}$ nanocages, we analyzed their band gap (E_g). The electronic sensitivity value (ΔE_g) for the interaction between FAV drug and pure $B_{12}N_{12}$ or Cu-modified $B_{12}N_{12}$ nanocages was calculated as Eq. (3);

$$\Delta E_g = \left[\frac{\left(E_{gap(nanocage-FAV)} - E_{gap(nanocage)}\right)}{E_{gap(nanocage)}}\right] \times 100\% \quad (3)$$

where ΔE_g denotes the electronic sensitivity value, $E_{g(nanocage\text{-}FAV)}$ stands for the band gap of $B_{12}N_{12}$-FAV or Cu-modified $B_{12}N_{12}$-FAV complexes, $E_{g(nanocage)}$ is the band gap of pure $B_{12}N_{12}$ or Cu-modified $B_{12}N_{12}$ nanocages respectively.

The E_{ads} value for the interaction between FAV drug molecule and $B_{12}N_{12}$ or Cu − modified $B_{12}N_{12}$ nanocages were calculated as following Eqs. 4–6;

$$E_{ads} = E_{(nanocage-FAV)} - \left(E_{(nanocage)} + E_{(FAV)}\right) \quad (4)$$

$$E_{ads,CP} = E_{ads} + E_{BSSE} \quad (5)$$

$$E_{int} = E_{Nanocage-FAV} - \left(E_{FAV\ in\ complex} + E_{nanocage\ in\ complex}\right) \quad (6)$$

where $E_{(nanocage\text{-}FAV)}$ is the energy of the FAV-bonded $B_{12}N_{12}$ or Cu-modified $B_{12}N_{12}$ complexes, $E_{(nanocage)}$ is the energy of pure $B_{12}N_{12}$ or Cu-modified $B_{12}N_{12}$ nanocages, $E_{(FAV)}$ is the energy of the FAV drug molecule and E_{BSSE} is the basis set superposition error(BSSE). Also E_{int} denotes the interaction energy. For the interaction energy, $E_{FAV\ in\ complex}$ and $E_{nanocage\ in\ complex}$ refer to the energies of the FAV and $B_{12}N_{12}$ based on their respective coordinates in the optimized FAV•••Cu-modified $B_{12}N_{12}$ complexes. The BSSE-corrected adsorption energy was computed using the counterpoise (CP) method, following the approach established by Boys and Bernadi [90]. Assessing electronic charge transfer (Q_{CT}) meant analyzing the charge difference between FAV molecules adsorbed onto $B_{12}N_{12}$ or Cu-$B_{12}N_{12}$ and the unbound FAV drug, which was estimated as Eq. (7);

$$Q_{CT} = Q_{(nanocage-FAV)} - Q_{(FAV)} \quad (7)$$

where $Q_{(nanocage\text{-}FAV)}$ and $Q_{(FAV)}$ represent the charges of FAV molecule adsorbed on $B_{12}N_{12}$ or Cu-modified nanocages and isolated FAV drug, respectively.

Quantum molecular descriptors such as the electrophilicity index (ω), electronic chemical potential (μ), chemical softness (S), and chemical hardness (η) were calculated using equations 10–13 [61]. The effect of water solvents on FAV drug interactions with adsorbents is analyzed using a self-consistent reaction field (SCRF) method within the conductor-like polarizable continuum model (CPCM) [91,92].

GaussSum, a valuable tool, was employed to generate density of states (DOS) [93] spectra, offering comprehensive insights into the orbital composition. This approach aids in visualizing the distribution and composition of orbitals, allowing for a better understanding of electronic structures.

To visualize the non-covalent interactions (NCI) between the drug and the adsorbent, we utilized the VMD [94] program. Additionally, the analysis of reduced density gradient (RDG) was conducted using the Multiwfn 3.7 [95] software. Shamsa Bibi *et al.* used the DFT B3LYP method with 6-31G(d,p) basis set without dispersion correction to calculate non-covalent interactions (NCI) [96]. These methodologies enable us to gain a comprehensive understanding of the charge distribution, orbital composition, and the nature of non-covalent interactions between the drug and the adsorbent.

3. Results and Discussion

3.1. Structural, electronic properties and adsorption site analyses

The optimized $B_{12}N_{12}$ nanocage, obtained using the B3LYP/6-311G (d,p) basis set, is illustrated in Fig. 1a. The $B_{12}N_{12}$ nanocage is highly stable, with equivalent nitrogen and boron sites. It consists of six tetragonal (4-membered) rings and eight hexagonal (6-membered) rings. The B-N bond lengths vary depending on their positions. The

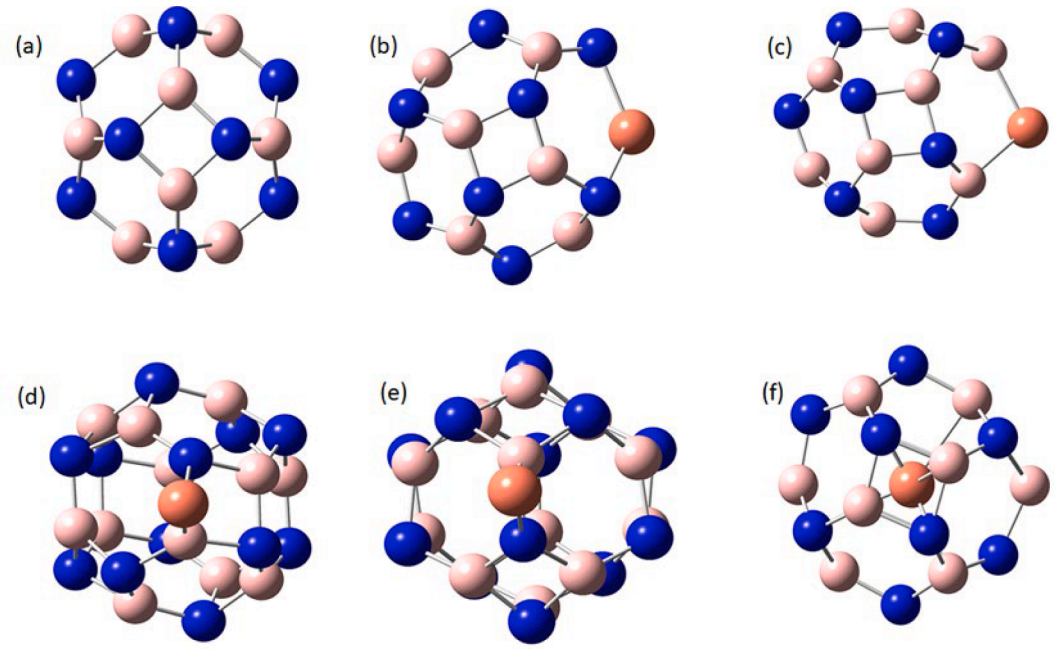

Fig. 1. Optimized structures for (a) isolated $B_{12}N_{12}$, (b) $CuB_{11}N_{12}$, (c) $B_{12}N_{11}Cu$,(d)Cu@b64(e) Cu@b66, and (f) Cu@$B_{12}N_{12}$ nanocages.

optimized B-N bond length of pristine $B_{12}N_{12}$ between two hexagonal rings (b66) is 1.438 Å, while the B-N bond between a tetragonal and a hexagonal ring (b64) is 1.486 Å. These findings are consistent with previous theoretical research studies [97–99].This study explored various sites for modifying Cu on $B_{12}N_{12}$ nanocages, including doped, decorated, and encapsulated configurations. The sites were designated as follows: (i) doped $CuB_{11}N_{12}$, (ii) doped $B_{12}N_{11}Cu$, (iii) b_{66} (Cu decoration between two hexagonal rings), (iv) b_{64} (Cu placement between a tetragonal and hexagonal ring), (v) B_{top} (Cu positioning on boron top), (vi) N_{top} (Cu placement on nitrogen top), (vii) r_6 (Cu positioning on the center top of the hexagonal ring), and (viii) r_4 (Cu placement on top of the tetragonal ring). Despite attempts at all mentioned positions, five optimized structures were achieved: doped configurations ($CuB_{11}N_{12}$ and $B_{12}N_{11}Cu$, involving the substitution of a B and N atom with a Cu atom, respectively), decorated structures (Cu@b_{66} and Cu@b_{64}, where a Cu atom is positioned on the bond between two hexagonal rings and between a tetragonal and hexagonal ring, respectively), and an encapsulated structure (Cu@$B_{12}N_{12}$, with a Cu atom positioned within the $B_{12}N_{12}$ nanocage). Some other initial input geometries like Cu on top of B and N atom transformed into these final configurations during the optimization process. Fig. 1b and c exhibit the Cu-doped nanocages, $CuB_{11}N_{12}$ and $B_{12}N_{11}Cu$, respectively. Substituting either a B or N atom with a Cu atom resulted in structural deformation in the initial $B_{12}N_{12}$ nanocage. The protrusion of the Cu atom from the nanocage surface was notable, which was attributed to its larger atomic radius compared to B and N atoms. In the optimized $CuB_{11}N_{12}$ nanocage, the longest Cu-B bond length was 1.898 Å, and the shortest Cu-B bond length was 1.874 Å. This effect was more pronounced in the $B_{12}N_{11}Cu$ nanocage. In $B_{12}N_{11}Cu$, the longest Cu-B bond length was 2.038 Å, and the shortest Cu-B bond length was 1.936 Å. Fig. 1d and e depict two potential copper-decorated structures: Cu@b_{64} (Cu bonded between a hexagonal and a tetragonal ring) and Cu@b_{66} (Cu bonded between two hexagonal rings), respectively. In Cu@b66, the longest B-N bond length was 1.511 Å, 0.073 Å greater than in pure $B_{12}N_{12}$. In Cu@b64, the longest bond length was 1.596 Å, 0.004 Å longer than in the pristine structure. Fig. 1f illustrates the Cu atom encapsulated within a $B_{12}N_{12}$ nanocage (Cu@$B_{12}N_{12}$), showcasing B−N bond lengths (b_{66} = 1.427 Å and b_{64} = 1.482 Å) signifying the Cu atom's perfectly housed inside the $B_{12}N_{12}$ nanocage [89,100]. The bond lengths (b66 and b64) deviate slightly from those of the original pristine $B_{12}N_{12}$ nanocage. The results in Table 1 indicate that the optimized $B_{12}N_{12}$ nanocage structures exhibited a zero dipole moment and an E_g of 6.74 eV, which is consistent with previous theoretical research [98,101]. The E_{coh} values of the five Cu-modified nanocages ($CuB_{11}N_{12}$, $B_{12}N_{11}Cu$, Cu@b66, Cu@b64, and Cu@$B_{12}N_{12}$) were −7.05, −6.94, −7.08, −7.08, and −6.87 eV respectively, compared to −7.32 eV for the pristine $B_{12}N_{12}$ nanocage. Therefore, the $B_{12}N_{12}$ nanocage with an E_{coh} value of −7.32 eV demonstrates greater stability than the five copper-modified nanocages. However, despite the negative E_{coh} values, the Cu-modified $B_{12}N_{12}$ nanocages are feasible and viable. Similar findings were noted in the doping of $B_{12}N_{12}$ with Mn and Fe, [18] and the encapsulation of 3d, 4d, or 5d transition metal (TM) atoms within a $B_{12}N_{12}$ nanocage [100]. Nonetheless, we observed a significant decrease in E_g values ranging from 1.82 to 3.33 eV upon Cu-modification. These results align with prior research on Cu-decorated $B_{12}N_{12}$ nanocages, [17,102] the doping of $B_{12}N_{12}$ with Al, Ga, and Sc, [98] and the encapsulation of Fe, Co, Ni, Cu, and Zn atoms in the $B_{12}N_{12}$ nanocage [89]. Among the five Cu-modified systems, the $CuB_{11}N_{12}$-doped nanocage exhibited the most prominent band gap change. Conversely, an increase in the dipole moment was observed, ranging from 2.05 to 3.17 D, with a more pronounced effect seen in the Cu@$B_{12}N_{12}$ encapsulated nanocage. These modifications indicate varied interactions with the FAV molecule. Geometry optimization of $B_{12}N_{12}$ and Cu-modified $B_{12}N_{12}$ nanocages with the FAV drug was conducted to assess their potential as drug delivery carriers, employing MEP and adsorption energy calculations to identify active sites and interaction mechanisms with FAV. We explored the

Table 1
Calculated Values of Cohesive Energy(E_{coh}), Dipole Moment(μ_D), HOMO Energy (E_H), LUMO Energy(E_L), Band Gap(E_g) and Fermi Energy Level(E_F) for the Isolated Systems and Favipiravir Drug in gas phase.

System	E_{coh}(eV)	μ_D(Debye)	E_H(eV)	E_L(eV)	E_g(eV)	E_F(eV)
$B_{12}N_{12}$	−7.32	0.0	−7.85	−1.11	6.74	−4.48
$CuB_{11}N_{12}$	−7.05	2.05	−6.99	−5.17	1.82	−6.08
$B_{12}N_{11}Cu$	−6.94	2.34	−5.30	−2.49	2.81	−3.90
Cu@b64	−7.08	2.12	−4.93	−1.65	3.28	−3.29
Cu@b66	−7.08	2.20	−4.90	−1.57	3.33	−3.24
Cu@$B_{12}N_{12}$	−6.87	3.17	−4.28	−1.72	2.56	−3.0
FAV	–	3.25	−7.11	−2.57	4.54	−4.84

interaction between the FAV drug and the pristine $B_{12}N_{12}$ nanocage, examining various orientations (both vertical and horizontal). Ultimately, FAV aligns vertically in both initial orientations on the nanocage (Fig. S2).Through this exploration, we identified three distinct geometries, termed A1, A2, and A3 (Fig. 2), each showcasing a different orientation of the FAV drug on the $B_{12}N_{12}$ nanocage. We employed three different functionals, B3LYP, *w*B97XD and M06-2X, using the same basis set for the adsorption energy calculations. In the scenarios, the structure with the lowest energy corresponded to A1, demonstrating adsorption energies of −16.57, −24.22 and −24.18 kcal mol^{-1}(Table S1) respectively. In the B3LYP case, there is a slight deviation from the A2 geometry. In contrast, in the A3 geometry, the bond length between FAV and the $B_{12}N_{12}$ nanocage extends to 1.739 Å, resulting in a lower adsorption energy of −3.12 kcal mol^{-1}. The difference in adsorption energies is due to the increased distance between the oxygen (from the carbonyl group of FAV) and the $B_{12}N_{12}$ nanocage, as well as between the nitrogen from the benzene ring and the nanocage. Strong adsorptions usually occur at shorter distances, as seen in the A1 and A2 orientations. The O and N atoms also show negative MEP, indicating their tendency to interact with the positively charged B atoms of the $B_{12}N_{12}$ cage. Likewise, the N atom of $B_{12}N_{12}$ displays negative MEP, as shown in Fig. 2, is more relevant for the electrophilic attack by H atoms of FAV. This is supported by the average local ionization energy (ALIE) [103], which confirms these points as preferential sites for electrophilic attack. Based on MEP maps calculations and ALIE [103] analyses from the literature, different initial configurations of $B_{12}N_{12}$-FAV complexes were constructed by considering electrostatic attraction, with the resulting most stable complexes shown in Fig. 2.

Fig. 3 illustrates the labeled adsorption of FAV on the Cu-modified boron nitride nanocages, while Table S2 presents the calculated bond lengths before and after the interaction with the FAV drug. A significant hike in bond length was noted during the adsorption of FAV on the pristine $B_{12}N_{12}$ nanocage, from 1.58 Å to 1.68 Å. In the $CuB_{11}N_{12}$-FAV complex, the Cu_{13}-N_{30} bond increased from 1.83 Å to 1.98 Å, the N_1-O_{34} bond increased from 2.62 Å to 3.32 Å, while the N_{11}-H_{29} bond decreased slightly from 3.62 Å to 2.71 Å. Similarly, in the $B_{12}N_{11}$Cu-FAV complex, the Cu_{12}-N_{30} bond increased from 1.82 Å to 1.96 Å. In the Cu@b64-FAV and Cu@b66-FAV complexes, the bond lengths of Cu_{25}-N_{31} increased from 1.81 Å to 1.85 Å and 1.84 Å to 1.89 Å, respectively. The Cu@$B_{12}N_{12}$-FAV complex exhibited a notable decrease in the B_8-N_{31} bond length, decreasing significantly from 1.86 Å to 1.51 Å, indicating a decrement of 0.35 Å. These shifts in bond lengths indicate an enlargement within the complexes, reflecting heightened reactivity after adsorption. The optimized bond lengths in the interacting complexes followed a trend: Cu@b64-FAV∼Cu@b66-FAV (1.85 Å) < $B_{12}N_{11}$Cu-FAV (1.96 Å) < $CuB_{11}N_{12}$-FAV (1.98 Å). This pattern indicates that Cu@b64-FAV∼Cu@b66-FAV complexes exhibit moderate interaction distances of 1.85 Å, while $CuB_{11}N_{12}$-FAV∼$B_{12}N_{11}$Cu-FAV complexes show longer interaction bond lengths of 1.96 Å and 1.98 Å, respectively.

3.2. Analyses of FAV drug adsorption on Cu-modified $B_{12}N_{12}$ nanocages

To assess the capacity of both the pristine $B_{12}N_{12}$ and its copper Cu-modified nanocages as carriers for the delivery of FAV drug, we performed adsorption energy calculations both in gas phase and solvent phase utilizing density functional theory (DFT) at the B3LYP/6-311G(d, p) basis set. Fig. 3 illustrates the stable configurations of the FAV drug adsorbed on Cu-modified $B_{12}N_{12}$ nanocages. The calculated adsorption energies of Cu-modified boron nitride nanocages ($CuB_{11}N_{12}$, $B_{12}N_{11}$Cu, Cu@b64, Cu@b66, and Cu@$B_{12}B_{12}$) are presented in Table 2. Earlier studies by Mohsen Asle Zaeem *et al.* [104] and Tanveer Hussain *et al.* [105] characterized an E_{ads} value of ± 1 eV (±23 kcal mol^{-1}) as weak chemisorption or strong physisorption. In this study aimed at drug delivery of FAV in biosystems, strong physisorption was observed in $CuB_{11}N_{12}$-FAV and $B_{12}N_{11}$Cu-FAV complexes, while Cu@b64-FAV, Cu@b66-FAV, and Cu@$B_{12}N_{12}$-FAV complexes showed chemisorption interactions. This indicates that the Cu-modified $B_{12}N_{12}$ nanocages exhibit strong adsorption of the FAV drug, demonstrating their potential for drug delivery. The negative values of E_{ads} observed for all drug-delivery complexes, affirm the stable adsorption of various FAV drug orientations on the Cu-modified $B_{12}N_{12}$ nanocages. The adsorption energy ranged from −20.41 to −56.58 kcal mol^{-1} and the trend was Cu@$B_{12}N_{12}$-FAV>Cu@b66-FAV>Cu@b64-FAV>$B_{12}N_{11}$Cu-FAV>$CuB_{11}N_{12}$-FAV respectively. The highest adsorption of −56.58

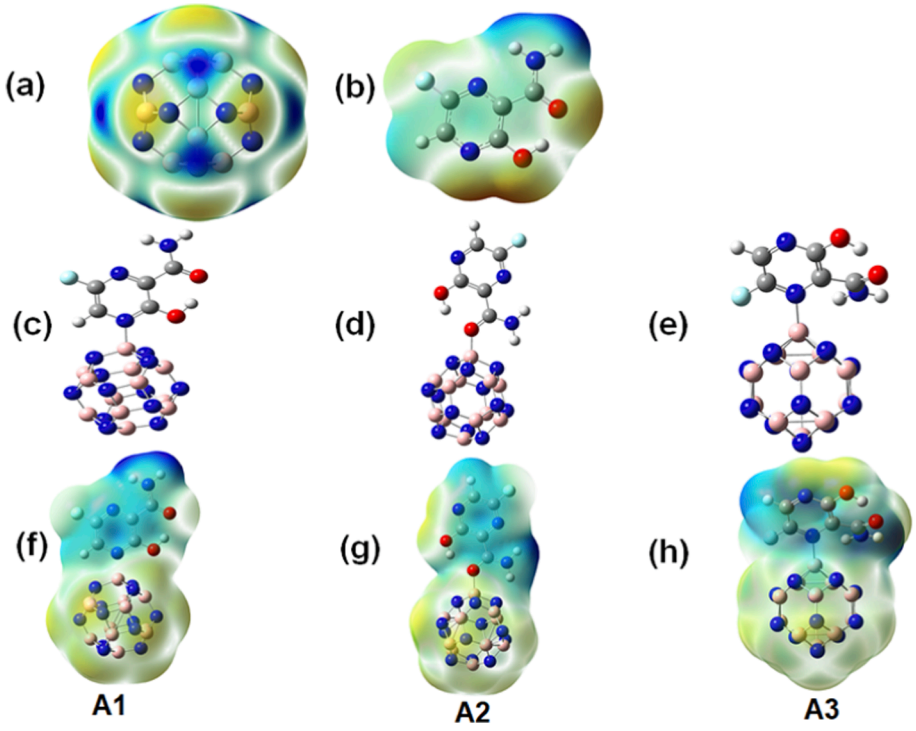

Fig. 2. Representations of MFP of $B_{12}N_{12}$ (a), MEP of FAV drug (b); optimized structures of A1(c), A2 (d), A3 (e); and MEPs of A1 (f), A2 (g) and A3 (h).

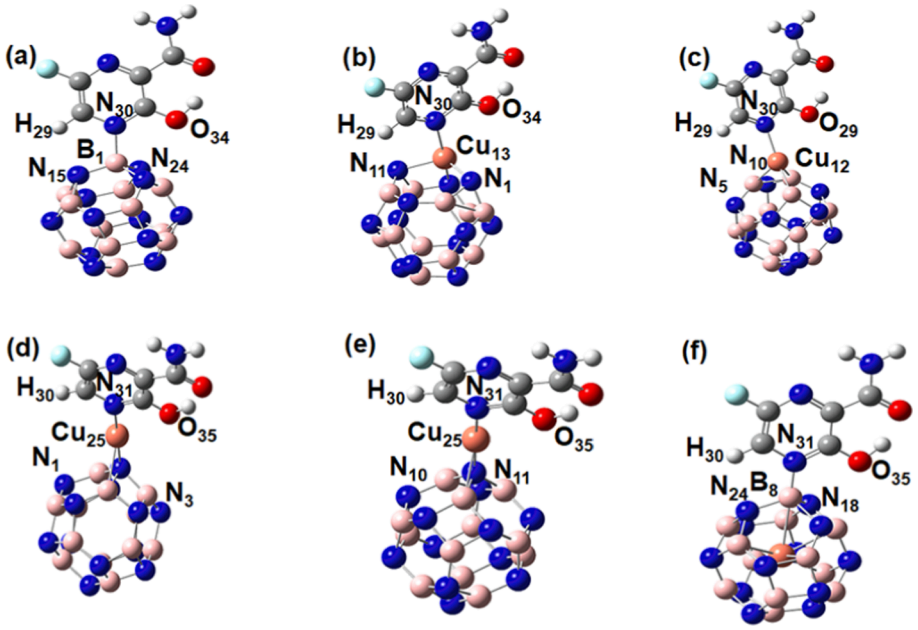

Fig. 3. Representations of the optimized complexes between FAV drug and isolated nanocages with labeling (a) $B_{12}N_{12}$-FAV (b) $CuB_{11}N_{12}$-FAV, (c) $B_{12}N_{11}Cu$-FAV, (d) Cu@b64-FAV, (e) Cu@b66-FAV, and (f) $Cu@B_{12}N_{12}$-FAV.

Table 2
Calculated Bond Lengths (Å) after adsorption of FAV, Interaction Energy(E_{int}), Adsorption Energy(E_{ads}), BSSE-corrected adsorption energy(E_{BSSE}), Enthalpy Change (ΔH), Gibbs free Energy(ΔG) in kcal mol^{-1} and change in entropy(ΔS) in kcal mol^{-1}K^{-1}, of all the Studied Complexes using the Optimized Structures Obtained from the B3LYP/6-311G(d,p) basis set in gas phase.

systems	$d_{cage\text{-}N}$ (Å)	E_{int} kcal mol^{-1}	E_{ads} kcal mol^{-1}	E_{BSSE} kcal mol^{-1}	ΔH kcal mol^{-1}	ΔG kcal mol^{-1}	ΔS kcal mol^{-1}K^{-1}
$B_{12}N_{12}$-FAV	1.683	−28.74	−16.57	−13.10	−16.35	−4.78	−0.039
$CuB_{11}N_{12}$-FAV	1.983	−25.97	−20.41	−11.39	−15.83	−13.19	−0.009
$B_{12}N_{11}Cu$-FAV	1.960	−30.14	−28.61	−19.29	−28.05	−17.25	−0.036
Cu@b64-FAV	1.841	−53.89	−45.61	−28.92	−45.07	−33.74	−0.038
Cu@b66-FAV	1.849	−54.33	−45.68	−28.98	−45.14	−33.89	−0.038
$Cu@B_{12}N_{12}$-FAV	1.512	−65.26	−56.58	−52.41	−56.32	−43.26	−0.044

kcal mol^{-1} occurs in the $Cu@B_{12}N_{12}$-FAV complex, while the smallest, −20.41 kcal mol^{-1}, occurs in the $CuB_{11}N_{12}$-FAV complex.

The BSSE-corrected adsorption energy was calculated using the counterpoise (CP) formalism according to the Boys and Bernardi method [90].The BSSE energies of Cu-modified $B_{12}N_{12}$-FAV complexes, ranging from 4.17 to 16.71, are detailed in Table S3. The BSSE energies of the complexes $CuB_{11}N_{12}$-FAV, $B_{12}N_{11}Cu$-FAV, Cu@b64-FAV, Cu@b66-FAV and $Cu@B_{12}N_{12}$-FAV are 9.02, 9.32, 16.71, 16.69 and 4.17 kcal mol^{-1} respectively. In this study, the adsorption energy and BSSE-corrected adsorption energy were also calculated using the M06-2X/6-311G(d,p) basis set and are summarized in Table S4. The computed E_{ads} and BSSE-corrected energies (E_{BSSE}) are shown in Table 2, ranging from −21.41 to −56.58 kcal mol^{-1} and −11.39 to −52.41 kcal mol^{-1}, respectively. The FAV drug adsorption energies on original and Cu-modified $B_{12}N_{12}$ nanocages($CuB_{11}N_{12}$-FAV, $B_{12}N_{11}Cu$-FAV, Cu@b64-FAV, Cu@b66-FAV and $Cu@B_{12}N_{12}$-FAV) are −16,57, −20.41, −28.61, −45.61, −45.68, and −56.58 kcal mol^{-1} respectively. Modified nanocages usually exhibit improved drug adsorption compared to the original, with the exception of the Cu-doped ones. Fig. 4 illustrates the adjustment between ZPE-adsorption energy and BSSE-corrected energy, emphasizing the contributions from doped transition metals. Reviews [106,107] indicate that lower negative BSSE-corrected adsorption energies suggest more favorable drug-cage interactions.

The adsorption process increased by incorporating a Cu atom on the $B_{12}N_{12}$ nanocages. The results in Table 2 show that the adsorption of the FAV drug onto Cu-modified $B_{12}N_{12}$ nanocages occurred spontaneously (negative ΔG values) and was exothermic (negative ΔH values). The E_{ads}

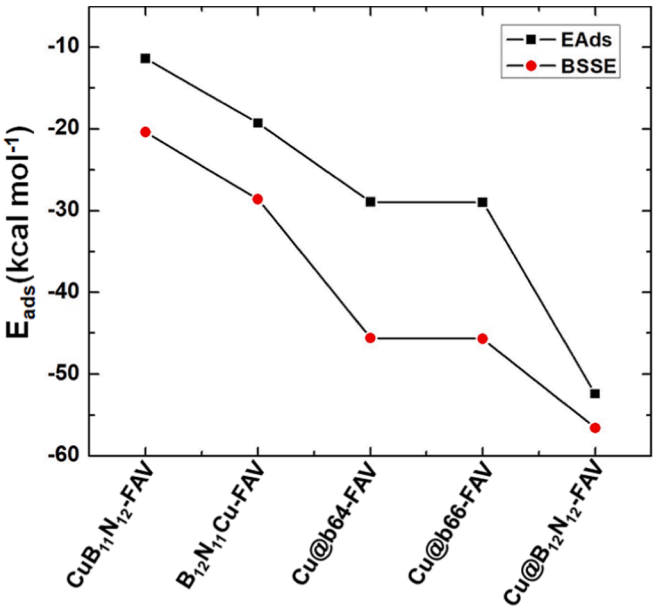

Fig. 4. Calculated ZPE-corrected adsorption energy *vs* BSSE-corrected adsorption energy at the B3LYP/6–311++G (d,p) level of theory.

values for the $B_{12}N_{11}Cu$-FAV, Cu@b64-FAV, Cu@b66-FAV, and Cu@$B_{12}N_{12}$-FAV complexes exceeded 27.21 kcal mol^{-1}, indicating a more negative range and limiting their sensor applicability, unlike the $CuB_{11}N_{12}$ nanocage. The $CuB_{11}N_{12}$ nanocage exhibited an E_{ads} value (−20.41 kcal mol^{-1}) between −8.16 kcal mol^{-1} and −27.21 kcal mol^{-1}[108] suggesting a moderate interaction with FAV drug, making it suitable as a drug carrier. Thus, the Cu-doped $CuB_{11}N_{12}$ nanocage interacts with the FAV drug molecule through a strong physisorption (weak chemisorption) process, indicating favorable adsorption–desorption behavior with a reasonable recovery time. The deformation energy of the complexes was calculated and summarized in Table S3, showing positive values and indicating distortion from the relaxed state. The electronic structure of the FAV drug after adsorption was also checked, with the HOMO at −7.03 eV and LUMO at −2.52 eV, resulting in an E_g of 4.51 eV. Before adsorption, the HOMO was −7.11 eV and the LUMO was −2.57 eV, with an E_g of 4.54 eV. This indicates no significant change in the FAV drug's electronic structure after adsorption on the studied nanocages, showing that the adsorption process did not significantly alter the drug's electronic properties.

To thoroughly examine the drug adsorption on nanocages, we computed the adsorption enthalpy (ΔH) and Gibbs free energy (ΔG) of the complexes under standard conditions (298.15 K and 1 atm). The negative ΔH and ΔG values indicate the spontaneity and exothermic nature of the adsorption process. The sequence of negative ΔG values ($CuB_{11}N_{12}$-FAV<$B_{12}N_{11}Cu$-FAV<Cu@b64-FAV<Cu@b66-FAV<Cu@$B_{12}N_{12}$-FAV) further highlights the spontaneous interaction between these Cu-modified $B_{12}N_{12}$ cages and FAV. Additionally, the study explored the potential of these nanomaterials as drug carriers.

3.3. Electronic properties

The analysis of electron densities and electronic energy levels provides crucial insights into the influence of Cu-modification and FAV adsorption on both the pristine and Cu-modified $B_{12}N_{12}$ nanocages. The optimized FAV adsorbed Cu-modified $B_{12}N_{12}$ nanocages are depicted in Fig. 5. Table 3 details essential orbital parameters, including HOMO and LUMO energies, Fermi level energy (E_F), and the HOMO-LUMO energy difference (E_g). The $B_{12}N_{12}$ nanocage demonstrates semiconductor characteristics with an E_g value of 6.74 eV. Specifically, it's HOMO and LUMO energies are recorded as −7.85 and −1.11 eV, respectively, with an E_F at −4.48 eV. The Fermi level energy denotes the midpoint of the HOMO-LUMO energy gap. Introducing Cu onto the $B_{12}N_{12}$ nanocage induces changes in the HOMO-LUMO energies [109]. In the $CuB_{11}N_{12}$ nanocage, the HOMO energy rises to −6.99 eV, the LUMO energy decreases to −5.17 eV, narrowing the HOMO-LUMO gap to 1.82 eV, with the Fermi level shifting to −6.08 eV. Conversely, in the $B_{12}N_{11}Cu$ nanocage, the HOMO energy increases to −5.30 eV, causing the LUMO energy to decrease to −2.49 eV, resulting in a reduced HOMO-LUMO gap of 2.81 eV, with the Fermi level registered at −3.90 eV. The changes in HOMO and LUMO energies are attributed to the stabilization of the LUMO and destabilization of the HOMO, respectively. In the decorated systems Cu@b_{66} and Cu@b_{64}, the HOMO energies are increased from −7.85 eV to −4.93 and −4.90 eV, while the LUMO energies decrease from −1.11 eV to −1.65 and −1.57 eV, respectively. This leads to energy gaps of 3.28 and 3.33 eV, with Fermi level energies at −3.29 and −3.24 eV, respectively. In the encapsulated configuration Cu@$B_{12}N_{12}$ nanocage, the HOMO and LUMO energies are noted as −4.28 eV and −1.72 eV, respectively. This results in an energy gap of 2.56 eV and a Fermi level energy of −3.00 eV respectively.

The investigation of the electronic characteristics of FAV interacting with Cu-modified adsorbent complexes involved an in-depth analysis of the HOMO, LUMO, and Frontier Molecular Orbitals (FMOs) depicted in Fig. 5. Notable changes in HOMO and LUMO energy levels were observed upon drug adsorption onto the nanocages, as shown in Fig. 5. The reduction in the HOMO energy level resulted in a decreased ionization energy, facilitating electron movement upon FAV drug adsorption. Initially, the HOMO and LUMO orbitals were uniformly distributed across the drug. After adsorption, the orbital distribution on the complex nanocages became non-uniform due to charge transfer. Post-adsorption, the HOMO was uniformly dispersed across the molecule, while the LUMO predominantly localized on the FAV, with a fraction shared between the adsorbent and the drug. Notably, a substantial distribution area between the FAV drug and the metal-doped adsorbent was evident in the HOMO and LUMO orbitals, indicating strong chemical bonds and robust interaction between the molecules. The analysis of Frontier Molecular Orbitals clarified the sensitivity and reactivity of the metal-doped adsorbent nanostructures. These insights guided computations for electron affinity (A=-E_{LUMO}) and ionization potential (I=-E_{HOMO}). The decrease in HOMO energy reduced the ionization potential, enhancing the complexes' reactivity. Conversely, the electron affinity increased with rising E_{LUMO}, signifying heightened reactivity, especially in $CuB_{11}N_{12}$-FAV. The adsorption of Cu on $B_{12}N_{12}$ nanocages shifted the

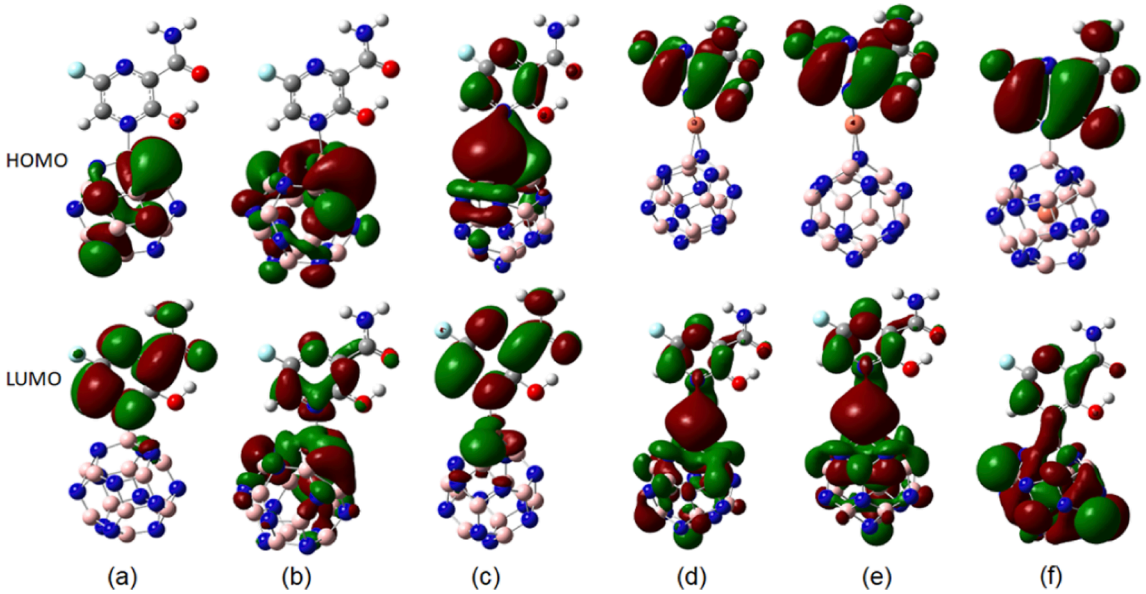

Fig. 5. Three–dimensional maps of the HOMO-LUMO electron distribution of the complexes (a) $B_{12}N_{12}$-FAV (b) $CuB_{11}N_{12}$-FAV, (c) $B_{12}N_{11}Cu$-FAV, (d) Cu@b64-FAV, (e) Cu@b66-FAV, and (f) Cu@$B_{12}N_{12}$-FAV.

Table 3
Calculated Values of Dipole Moment (Debye), HOMO Energy(E_H), LUMO Energy(E_L), Band Gap(E_g), Electronic Sensitivity(% ΔE_g), Fermi Energy Level(E_F) and the fractional charge transfer Q_{CT} (Q_{CT} for the complexes between FAV drug and Isolated Nanocages) in gas phase.

System	Dipole moment(Debye)	E_H(eV)	E_L(eV)	E_g(eV)	ΔE_g(%)	E_F(eV)	Q_{CT}
$B_{12}N_{12}$-FAV	10.90	−6.80	−3.85	2.96	56.08	−5.33	0.06
$CuB_{11}N_{12}$-FAV	10.16	−6.42	−3.41	3.01	65.38	−4.92	−0.13
$B_{12}N_{11}Cu$-FAV	5.65	−4.83	−3.03	1.80	35.94	−3.93	0.28
Cu@b64-FAV	5.39	−3.74	−2.20	1.54	53.04	−2.97	0.61
Cu@b66-FAV	5.71	−3.72	−2.13	1.59	52.25	−2.93	0.62
Cu@ $B_{12}N_{12}$-FAV	5.33	−4.01	−1.91	2.10	17.97	−2.96	0.57
FAV	3.25	−7.11	−2.57	4.54	–	−4.84	–

HOMO towards the copper, making the metal electron-rich. However, being electropositive, the metal could not retain the excess electrons, leading to their dispersion.The relationship between the HOMO−LUMO gap (E_g) and conductivity is described a correlation between high energy levels in the newly formed HOMO and conductivity [110].The calculations in this study show that LUMO energies decreased in the nanocage geometries compared to the pure $B_{12}N_{12}$ nanocage. After the adsorption of the FAV drug on Cu-modified $B_{12}N_{12}$ nanocages, there was a noticeable stabilization in both the HOMO and LUMO energies. The Fermi level energies for the $CuB_{11}N_{12}$-FAV, $B_{12}N_{11}Cu$-FAV, Cu@b64-FAV, Cu@b66-FAV, and Cu@$B_{12}N_{12}$-FAV geometries were determined as −4.92 eV, −3.93 eV, −2.97 eV, −2.93 eV, and −2.96 eV, respectively. The adsorption of FAV on Cu resulted in reduced interaction between Cu and the $B_{12}N_{12}$ nanocage, leading to a decrease in the push of outer d electrons due to decreased coordination with the metal center. In the FAV-Cu-$B_{12}N_{12}$ complex, the HOMO showed higher density on the metal with some diffuse density within the cage. Furthermore, the energies of the LUMO decreased upon FAV adsorption, indicating a shift towards the nanocage and contributing to its stabilization through reduced energy levels. The conductivity (σ) of $B_{12}N_{12}$ nanocage and its Cu-modified nanocages with the FAV drug can be determined as Eq. (8) as follows;

$$\sigma \propto \exp(-E_g/KT) \tag{8}$$

Where σ denotes the conductivity, E_g energy gap between HOMO-LUMO, K is the Boltzmann's constant and T is the temperature. This equation suggests a significant increase in electrical conductivity with the reduction in the HOMO−LUMO energy gap (E_g). Our findings highlight significant improvements in the Cu-doped $CuB_{11}N_{12}$ nanocage's sensing ability for FAV adsorption compared to pristine $B_{12}N_{12}$ nanocages and other modified nanocages. As shown in Table 3, the Q_{CT} is an essential indicator for evaluating charge transfer during adsorption. A Q_{CT} value below zero indicates charge transfer from the drugs to the carriers, while a Q_{CT} value above zero signifies charge transfer from the carriers to the drugs. In the studied complexes, all Q_{CT} values were greater than zero except for $CuB_{11}N_{12}$ nanocages, suggesting charge flowed from the surface to the drug in these cases [109]. The charge transfer amounts were 0.28 e, 0.61 e, 0.62 e, and 0.57 e for the complexes of $B_{12}N_{11}Cu$-FAV, Cu@b64-FAV, Cu@b66-FAV, and Cu@$B_{12}N_{12}$-FAV, respectively. In the case of $CuB_{11}N_{12}$, the transfer amount was −0.13 e, indicating that the drug acted as a charge donor. The higher Q_{CT} values of the doped systems compared to the original suggest that doping enhances the nanocarrier's charge transfer capability.

3.4. Dipole moment analysis

As evident from Table 3, the dipole moment of the FAV drug prior to adsorption is measured at 3.25 debye, signifying its polar nature. The dipole moments were assessed for pure $B_{12}N_{12}$, Cu-modified $B_{12}N_{12}$, and Cu-$B_{12}N_{12}$-FAV structures. The symmetrical nature of the pure $B_{12}N_{12}$ cage results in a zero dipole moment. Introducing Cu onto this $B_{12}N_{12}$ nanocage increases the dipole moment from zero to a range of 2.05 to 3.17 D. This shift is attributed to the presence of Cu, disrupting the charge separation within $B_{12}N_{12}$ nanocages. For FAV-adsorbed Cu-modified $B_{12}N_{12}$ complexes, dipole moments range between 5.33 and 10.16 D. The change in dipole moment upon FAV adsorption on Cu-modified $B_{12}N_{12}$ nanocages originates from charge transfer between drugs and nanocages, leading to a greater deviation in the positive and negative charge centers of the complex compared to the isolated system. Consequently, the dipole moment of the complex is increased. Furthermore, the enhanced dipole moment indicates that the adsorption on the nanocage surface facilitates more efficient drug transport within the body. The most significant change in dipole moment is observed when FAV is adsorbed on $CuB_{11}N_{12}$nanocage (10.16 D), while the encapsulated Cu@$B_{12}N_{12}$-FAV shows the lowest dipole moment change (5.33 D). It is important to highlight that the incorporation of Cu in the system ($CuB_{11}N_{12}$) not only amplifies the dipole moment of the complex but also significantly enhances the dipole moment of the drug molecules within the complex. This observation underscores the advantageous role of the Cu doping system in facilitating drug flow. The dipole moment trend among the FAV complexes follows as $CuB_{11}N_{12}$-FAV>Cu@b_{66}-FAV>$B_{12}N_{11}Cu$-FAV>Cu@b_{64} > Cu@$B_{12}N_{12}$.

3.5. Density of states (DOS)

The interaction between FAV and Cu-modified $B_{12}N_{12}$ nanocages was confirmed through density of states (DOS) and partial density states (PDOS) analysis, as illustrated in Fig. 6 and Fig. S3.This analysis effectively illustrates the change in the energy gap (E_g) upon FAV adsorption onto various Cu-modified nanocages. DOS analysis quantifies the availability of electron states at distinct energy levels, with lower values indicating fewer available states and higher values indicating more available states. The pronounced change in E_g values post-FAV adsorption on Cu-modified $B_{12}N_{12}$ nanocages is noteworthy. The E_g range refers to the electron excited states, indicating the energy required for outermost shell electrons to become charge carriers, which is crucial for assessing a system's electrical conductivity. The E_g decrease observed after FAV interaction with Cu-modified $B_{12}N_{12}$ nanocages shifted their behavior towards a semiconductor, as evident from the DOS analysis in Fig. 6.The DOS analysis indicated that drug molecules mainly contributed to the HOMO, while the Cu-modified $B_{12}N_{12}$ nanocages exhibited higher values in the LUMO, actively engaging in the adsorption process via the LUMO orbital. The distribution of the LUMO orbital corresponds to the substantial contribution of the PDOS of FAV to the TDOS of the complexes. Comparing the LUMO values among various Cu-modified nanocages highlighted the significant contribution of the Cu-doped complex to the adsorption process, implying its potential effectiveness as an electrochemical sensor. All nanocages exhibited bonding attributes within the DOS value range of 0.0 to −15 eV. Additionally, their Fermi energy level values were calculated as −5.29, −3.93, −2.97, −2.93, and −2.96 eV for Cu-modified $CuB_{11}N_{12}$-FAV, $B_{12}N_{11}Cu$-FAV, Cu@b64-FAV, Cu@b66-FAV, and Cu@$B_{12}N_{12}$-FAV complexes, respectively. These observations from DOS analysis provide crucial insights into the electrochemical behavior and adsorption characteristics of the Cu-modified nanocages interacting with the FAV drug.

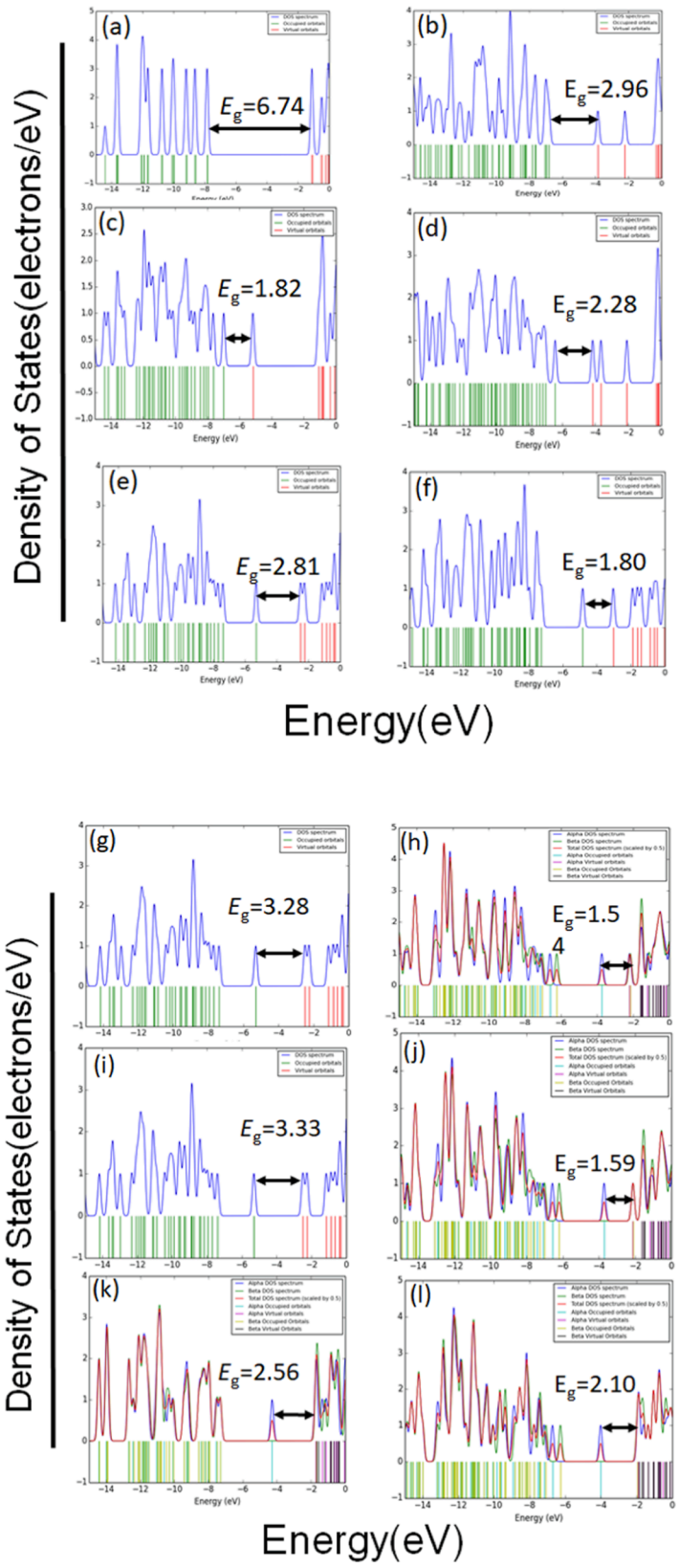

Fig. 6. Density of States (DOS) diagrams of isolated $B_{12}N_{12}$ (a), $CuB_{11}N_{12}$ (c), $B_{12}N_{11}Cu$ (e), Cu@b64 (g), Cu@b66 (i) and (k) Cu@$B_{12}N_{12}$ nanocages before and after interacting with Favipiravir ($B_{12}N_{12}$-FAV(b), $CuB_{11}N_{12}$-FAV(d), $B_{12}N_{11}Cu$-FAV (f), Cu@b64-FAV (h), Cu@b66-FAV(j), and Cu@$B_{12}N_{12}$-FAV(l)).

3.6. Global Indices of reactivity

Further investigation into the stability and reactivity of the complexes was conducted using global reactivity descriptors: ionization potential (*IP*), electron affinity (*EA*), chemical potential (μ), global hardness (η), electrophilicity index (ω), and global softness (*S*). These descriptors, calculated via the B3LYP/6-311G(d,p) basis set and outlined in Table 4, offer crucial insights. In this study, the chemical descriptors were calculated using the HF/STO-3G level of theory also, and the data are summarized in Table S5. Global hardness (η) has been associated with a chemical species' resistance to deformation in an electric field, where lower values indicate higher reactivity and lower stability. Conversely, higher global softness (*S*) values often indicate increased reactivity but decreased stability. Elevated chemical potential (μ) values signify higher reactivity and lower stability. The electrophilicity index (ω) differentiates between strong and weak electrophiles. Before adsorption, the complexes displayed an increasing order of global hardness values: 0.91, 1.41, 1.64, 1.66, and 1.28 for Cu-modified $CuB_{11}N_{12}$, $B_{12}N_{11}Cu$, $Cu@b_{64}$, $Cu@b_{66}$, and Cu@ $B_{12}N_{12}$nanocages, respectively. Post-FAV adsorption, these values changed to 1.14, 0.90, 0.77, 0.80, and 1.05 eV for the aforementioned complexes, indicating their high reactivity and low stability. Global softness values ranged closely from 0.4386 to 0.6494 eV. The order of chemical potential values was observed as Cu $B_{11}N_{12}$-FAV>$B_{12}N_{11}$Cu-FAV>$Cu@b_{64}$-FAV>Cu@ $B_{12}N_{12}$-FAV>$Cu@b_{66}$-FAV, with values of − 5.29, −3.93, −2.97, −2.96, and − 2.93 eV, respectively. Strong electrophilic properties were identified in $CuB_{11}N_{12}$-FAV (12.27 eV), $B_{12}N_{11}$Cu-FAV (8.58 eV), and $Cu@b_{64}$-FAV (5.73 eV). While Cu-modification on $B_{12}N_{12}$ enhanced the electrophilicity index value, a slight reduction was observed in the Cu-doped nanocage. The calculated adsorption energy based on global descriptors ranked the complexes as $B_{11}N_{12}$-FAV>$B_{12}N_{11}$Cu-FAV>$Cu@b_{64}$-FAV>$Cu@B_{12}N_{12}$-FAV>$Cu@b_{66}$-FAV, showcasing their high reactivity and sensitivity. The lower electronegativity of the FAV drug compared to the Cu-modified adsorbent suggested an electron flow from FAV to the nanocages. Regarding FAV as the donor and the nanostructure adsorbent as the acceptor, the negative Q_{CT} values confirmed the electron transfer from the drug to the nanocage adsorbent.

3.7. NBO analysis

Natural bond orbital (NBO) analysis is a powerful tool for understanding intra- and intermolecular bonding, hybridization, and charge transfer following interactions between an adsorbate and adsorbents. This analysis involves converting atomic orbitals (AOs) into natural bond orbitals (NBOs) using natural atomic orbitals (NAOs) and natural hybrid orbitals (NHOs). It facilitates the delocalization of electrons from filled Lewis-type donor NBOs to empty non-Lewis-type acceptor NBOs, transforming delocalized molecular orbitals into localized ones. This transformation significantly reflects fundamental chemical bonding concepts. Stabilization energy (E^2), is the second order perturbation energy in a donor and acceptor interaction based on $n\rightarrow\sigma^*$ or $\sigma\rightarrow\sigma^*$ charge transfer. When FAV interacts with Cu-modified nanocages the highest E^2 values are observed for charge transfer from lone pair of nitrogen atom of FAV to antibond pair or anti lone pair of Cu which ranges from 36.03 to 41.62 kcal mol^{-1}. For the $CuB_{11}N_{12}$-FAV, the E^2 value is 39.08 kcal mol^{-1} for $n_{(N30(FAV))} \rightarrow \sigma^*_{(Cu13)}$.For $B_{12}N_{11}$Cu-FAV, the E^2 value is 36.03 kcal mol^{-1} for $n_{(N30(FAV))} \rightarrow \sigma^*_{(Cu12\text{-}B20)}$. The highest value of E^2 for Cu@b64-FAV is 36.55 kcal mol^{-1} for $n_{(N31(FAV))} \rightarrow n^*_{Cu25}$ and for Cu@b66-FAV 41.62 kcal mol^{-1} for $n_{N31FAV}\rightarrow n^*_{Cu25}$. However, in $Cu@B_{12}N_{12}$-FAV complex, the charge transfer occurs for $\sigma \rightarrow \sigma^*$. The E^2 values for bond formation between nitrogen atom of FAV and boron atom of nanocages are 3.11, 3.11, 2.17 and 2.15 kcal mol^{-1} for $\sigma_{(C26\text{-}N31\ (FAV))} \rightarrow \sigma^*_{(B8\text{-}N18\ (nanocage))}$, $\sigma_{(C26\text{-}N31(FAV))} \rightarrow \sigma^*_{(B8\text{-}N19(nanocage))}$, $\sigma_{(C26\text{-}N31\ (FAV))} \rightarrow \sigma^*_{(B8(nanocage)\text{-}N31(FAV))}$ and $\sigma_{(C27\text{-}N31(FAV))} \rightarrow \sigma^*_{(B8(nanocage)\text{-}N31\ (FAV))}$, respectively. When FAV interacts with pristine $B_{12}N_{12}$, charge transfer occurred for $\sigma_{(B6\text{-}N24(nanocage))} \rightarrow \sigma^*_{(B1(nanocage)\text{-}N30(FAV))}$ and $\sigma_{(C25\text{-}N30(nanocage))} \rightarrow \sigma^*_{(B1(nanocage)\text{-}N30(FAV))}$ with the E^2 value of 15.24 and 3.65 kcal mol^{-1}, respectively. Table S6 presents second-order perturbation interaction energies between filled and empty NBOs, emphasizing substantial charge transfer within intermolecular NBOs.

3.8. Sensor mechanisms

Measuring the work function (Φ) holds pivotal importance in the construction of a drug sensing device. Mollania *et al.* [111], Mirhaji *et al.* [112] and Cachaneski-Lopes and Batagin-Neto [113] have established the work function as the minimum energy essential to release the least bound electron from a solid surface's Fermi energy level, extending toward a vacuum point. This parameter is pivotal for understanding the sensitivity and reactivity of doped boron nitride ($B_{12}N_{12}$) concerning FAV drugs. Assessing the conducting energy of a sensor material involves considering both the highest and lowest molecular orbital energy gap (E_g) alongside the work function of the sensing material (Φ). A reduced E_g value signifies the material's efficacy in electron transportation between the conduction and valence bands and the calculation is obtained using Eq. (9);

$$\Phi = V_{el(+\infty)} - E_F \tag{9}$$

The work function (Φ) is determined by the equation $\Phi = -E_F$, where $V_{el(+\infty)}$ represents the vacuum electrostatic potential energy (often approximated as close to 0), and E_F signifies the Fermi level energy. This equation establishes a direct relationship between the work function and the negative value of the Fermi energy. Thus, any fluctuation in the Fermi energy level induces a corresponding change in the work function, as highlighted in Table 5.

Research conducted by Dushman [114] has indicated that changes in

Table 4
The Energy gap(E_g), Ionization Potential(*IP*), Electron Affinity(*EA*), Chemical Potential(μ),Electrophilic Index(ω), Chemical Hardness(η), Chemical Softness(σ) and Electronegativity(χ) calculated for all systems. All units are electron volt (eV) calculated at B3LYP/6-311G(d,p) basis set in gas phase.

Systems	E_g	*IP*	*EA*	μ	ω	η	σ	χ
FAV	4.54	7.11	2.57	−4.84	5.16	2.27	0.2203	4.84
$B_{12}N_{12}$	6.74	7.85	1.11	−4.48	2.08	3.37	0.1484	4.48
$CuB_{11}N_{12}$	1.82	6.99	5.17	−6.08	20.31	0.91	0.5495	6.08
$B_{12}N_{11}Cu$	2.81	5.30	2.49	−3.90	5.41	1.41	0.3559	3.90
Cu@b64	3.28	4.93	1.65	−3.28	3.28	1.64	0.3049	3.28
Cu@b66	3.33	4.90	1.57	−3.24	3.15	1.66	0.3003	3.24
$Cu@B_{12}N_{12}$	2.56	4.28	1.72	−3.0	3.52	1.28	0.3906	3.0
$B_{12}N_{12}$-FAV	2.96	6.80	3.85	−5.33	9.60	1.48	0.3378	5.33
$CuB_{11}N_{12}$-FAV	3.01	6.42	3.41	−4.92	8.04	1.51	0.3322	4.92
$B_{12}N_{11}Cu$-FAV	1.80	4.83	3.03	−3.93	8.58	0.90	0.5556	3.93
Cu@b64-FAV	1.54	3.74	2.20	−2.97	5.73	0.77	0.6494	2.97
Cu@b66-FAV	1.59	3.72	2.13	−2.93	5.40	0.80	0.6289	2.93
$Cu@B_{12}N_{12}$-FAV	2.10	4.01	1.91	−2.96	4.17	1.05	0.4762	2.96

Table 5
Values of Electronic Sensitivity (% ΔE_g), Fermi Level Energy (E_F), Work Function (Φ), Changes in Work Function (%$\Delta\Phi$) and calculated NBO charges on Cu on the nanocages calculated using B3LYP/6-11G(d,p) basis set in gas phase.

System	ΔE_g(%)	E_F(eV)	Φ(eV)	% $\Delta\Phi$	Q(e) on Cu
$B_{12}N_{12}$		−4.48	4.48		
$CuB_{11}N_{12}$		−6.08	6.08		1.255
$B_{12}N_{11}Cu$		−3.90	3.90		0.848
Cu@b64		−3.29	3.29		0.470
Cu@b66		−3.24	3.24		0.455
$Cu@B_{12}N_{12}$		−3.0	3.00		1.033
$B_{12}N_{12}$-FAV	56.08	−5.33	5.33	–	–
$CuB_{11}N_{12}$-FAV	65.38	−4.92	5.29	−12.99	1.352
$B_{12}N_{11}Cu$-FAV	35.94	−3.93	3.93	0.77	1.022
Cu@b64-FAV	53.04	−2.97	2.97	−10.77	0.964
Cu@b66-FAV	52.25	−2.93	2.93	−9.57	0.962
Cu@ $B_{12}N_{12}$-FAV	17.97	−2.96	2.96	−1.33	1.045
FAV	–	−4.84	4.84	–	–

the work function of a semiconductor, observed using the Kelvin probe method, affect the emission of electron current densities from the surface. This alteration in emission properties within an electric field generates electric signals, facilitating the detection and identification of specific chemical species. The Richardson − Dushman equation further elucidates the strong correlation between the work function and the emitted electron current density (j) from the solid surface, expressed mathematically as Eq. (10);

$$j = AT^2\exp\left(\frac{-\Phi}{KT}\right) \tag{10}$$

Equation (10) involves a complex formulation for precise calculations and is defined as follows: A represents the Richardson constant (A/m^2), k denotes Boltzmann's constant, j signifies current density, and T stands for temperature (K). To compute the change in Φ after the adsorption of FAV drugs, it is determined using Eq. (11);

$$\Delta\Phi = \left(\frac{\Phi_2 - \Phi_1}{\Phi_1}\right) \times 100\% \tag{11}$$

Where Φ_1 and Φ_2 are the values of Φ for the doped $B_{12}N_{12}$ and the FAV drug/doped $B_{12}N_{12}$ nanocomplex, respectively.

Table 5 displays the work function values for isolated doped nanocages before drug adsorption, ranging from 3.00 to 6.08 eV. After drug adsorption, these values decreased, falling within the range of 2.96 to 5.29 eV. This decrease implies an electron flow from the FAV drug to the modified $B_{12}N_{12}$ nanocage and then to the adsorbed complexes. As a result of this charge transfer, the energy gap reduced post-adsorption. The modified nanocages exhibited varying changes upon interaction with FAV, showcasing percentage changes of 65.38 %, 53.04 %, 52.25 %, 35.94 %, and 17.97 % for $CuB_{11}N_{12}$-FAV, $Cu@b_{64}$-FAV, $Cu@b_{66}$-FAV, $B_{12}N_{11}Cu$-FAV, and $Cu@B_{12}N_{12}$-FAV respectively. These nanocages displayed lower energy gap values and higher percentage changes, indicating their potential as work function sensors for drug detection. Among them, the Cu-doped $CuB_{11}N_{12}$ nanocage showed higher sensitivity to the FAV drug.

The computation of the electron transfer fraction, offering an assessment of both the electronegativity of the interacting surface and the adsorbed complex, along with an evaluation of the chemical hardness within these interacting systems. This calculation provided valuable insights into the rate of electron charge transfer from the adsorbate to the adsorbent surfaces, shedding light on the strength of the charge interaction.

3.9. Non-covalent interaction analysis (NCI)

In the realm of drug design, NCI (Non-Covalent Interaction) analysis stands as a pivotal tool for understanding the different types of intra- and inter-molecular interactions between the adsorbate and adsorbent based on the electron density and its derivatives. To further confirm the interaction types between the FAV drug and transition metal Cu-modified $B_{12}N_{12}$ nanocages, we applied NCI analysis tool. The RDG plots which are generated by the reduced density gradient (RDG) S(r) versus electron density (ρ(r)) using Eq. (12);[115]

$$S(r) = \frac{1}{2(3\pi^2)^{1/3}}\frac{|\nabla\rho(r)|}{\rho(r)^{4/3}} \tag{12}$$

The 2D RDG scattered plots of studied nanocage complexes are displayed in Fig. 7. Within the NCI approach, the blue regions corresponding to large negative values of $(sign(\lambda_2)\rho)$, the second eigenvalue of the Hessian matrix (λ_2) with the electron density, indicating attractive interactions such as dipole–dipole or hydrogen bonding. The red regions with positive values signify nonbonding interactions and indicate steric hindrance [116]. When $(sign(\lambda_2)\rho) \approx 0$(depicted in green), it signifies very weak van der Waals (*vdW*) interaction. In Fig. 7a-–e, spikes are noticeable at low values of $(sign(\lambda_2)\rho)$, indicating weak interactions between FAV and Cu-modified $B_{12}N_{12}$ nanocages. However, in Fig. 7f, blue spikes emerge at large values of $(sign(\lambda_2)\rho)$, indicating strong interaction between FAV and Cu-modified nanocages. The red regions with positive values signify nonbonding interactions and indicate steric hindrance. Furthermore, in Fig. 8, 3D color-filled RDG isosurfaces of all studied complexes are depicted. In each complex, disk-like green–red isosurfaces are present in between FAV and nanocages, stabilizing the vertical alignment of FAV molecule during interaction with nanocage. Additionally, two disk-like isosurfaces are observed within the FAV molecules, between nitrogen and hydrogen atoms and oxygen and hydrogen atoms, indicating intramolecular hydrogen bonding. For comparison without dispersion, we also examined non-covalent interactions (NCI) with dispersion correction using the M06-2X/6-311G(d,p) level of theory. The calculated NCI results are illustrated in Figs. S4 and S5.

3.10. Solvent effect and recovery time

To explore the interaction between the Cu-modified $B_{12}N_{12}$ nanocages and the FAV drug for potential drug-delivery applications, we optimized the nanocage complexes in a water solvent using the polarizable continuum model (PCM).The impact of the solvent on the stability of the designed complexes was assessed by computing the solvation energy using the following Eq. (13);

$$E_{sol} = E_{water} - E_{gas} \tag{13}$$

Where E_{sol} denotes the solvation energy, E_{water} is the total energy of the complex in water media, while E_{gas} is the total energy in the gas phase. The solvation energy of the FAV drug adsorbed on the Cu-modified $B_{12}N_{12}$ nanocages exhibited a notable increase, confirming its solubility in water media and suggesting successful drug delivery to the target cell environment. Therefore, the determination of adsorption energies for the studied complexes in the aqueous phase provides valuable insights into their anticipated behavior within the human body. The interaction, adsorption, and solvation energies were calculated, as thoroughly explained in the computational methods section, and are compiled in Table 6.The water phase stability of the Cu-modified $B_{12}N_{12}$-FAV complexes is evident from Table 6, as indicated by the Favorable adsorption energies ($E^{ads}_{solvent}$) for all the examined complexes, ranging from −18.23 to −54.19 kcal mol^{-1}. The computed values of interaction energy, $E^{int}_{solvent}$ and adsorption energy, $E^{ads}_{solvent}$ in the water phase show a difference in order similar to that in the gas phase, making it less negative than in the gaseous phase. This difference can be attributed to variations in the energy of the deformed monomers.

The negative solvation energy value in water further indicates the stability of the investigated complexes. However, the $Cu@B_{12}N_{12}$-FAV

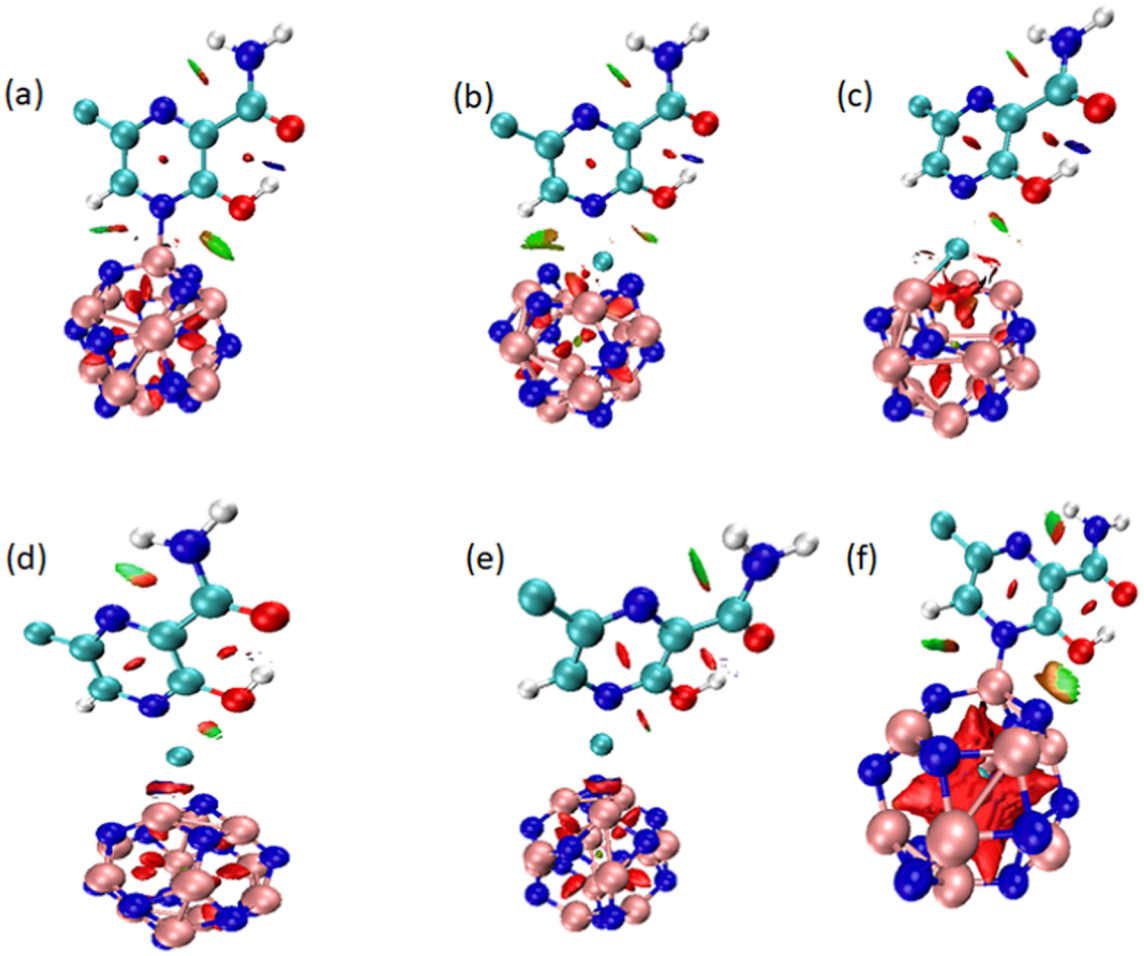

Fig. 7. 2D-RDG scatter plots of (a) $B_{12}N_{12}$-FAV, (b) $CuB_{11}N_{12}$-FAV, (c) $B_{12}N_{11}Cu$-FAV, (d) Cu@b64-FAV, (e) Cu@b66-FAV and (f) $Cu@B_{12}N_{12}$-FAV complexes.

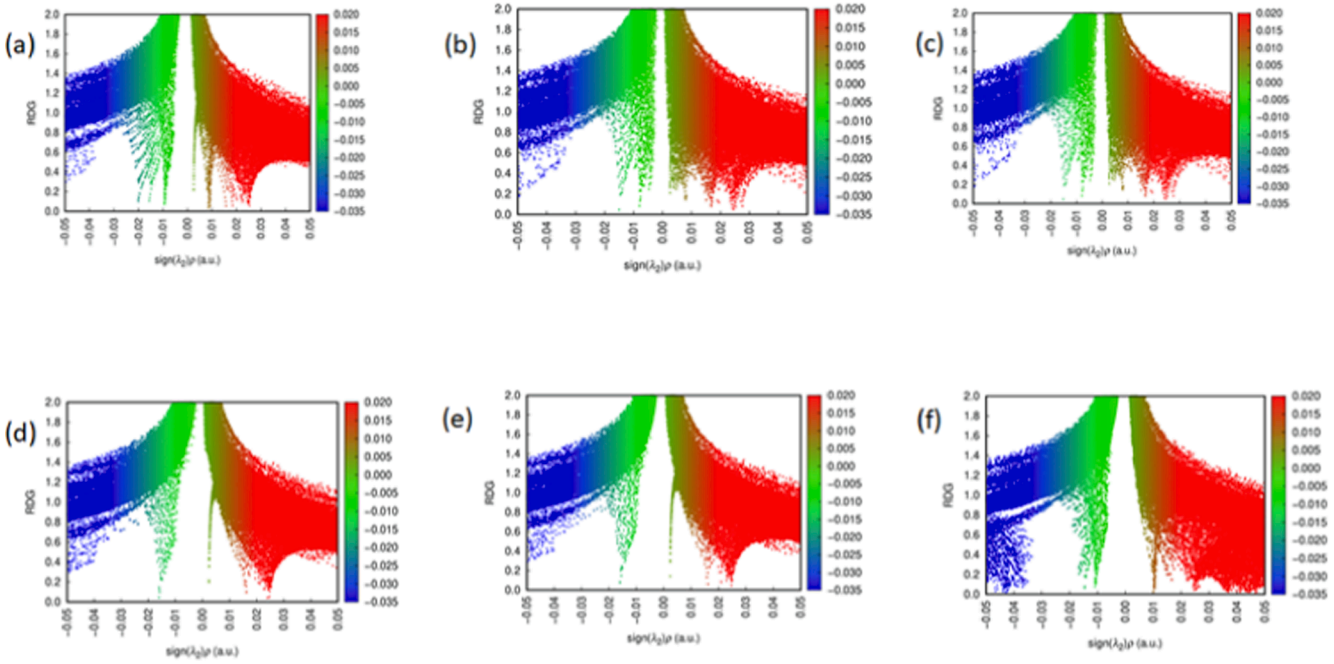

Fig. 8. The 3D color-filled *iso*-surface graphs for the studied complexes of a) $B_{12}N_{12}$-FAV, (b) $CuB_{11}N_{12}$-FAV, (c) $B_{12}N_{11}Cu$-FAV, (d) Cu@b64-FAV, (e) Cu@b66-FAV and (f) $Cu@B_{12}N_{12}$-FAV.

Table 6
Dipole Moment (Debye), Interaction energy ($E_{int}^{solvent}$) and adsorption energy ($E_{ads}^{solvent}$) in kcalmol^{-1} for the optimized complexes in water phase and solvation energy (ΔE_{sol} in kcalmol^{-1}) of FAV-Cu-modified $B_{12}N_{12}$ optimized complexes in water phase.

systems	DM(Debye)	$E_{int}^{solvent}$	$E_{ads}^{solvent}$	[a]ΔE_{sol}
$CuB_{11}N_{12}$-FAV	14.30	−23.09	−18.23	−12.48
$B_{12}N_{11}Cu$-FAV	9.75	−28.57	−24.61	−12.22
Cu@b64-FAV	10.50	−60.68	−44.55	−15.63
Cu@b66-FAV	10.26	−60.32	−45.12	−16.19
Cu@$B_{12}N_{12}$-FAV	7.68	−61.93	−54.19	−11.12

[a] $E_{sol} = E_{solvent}$-E_{gas}

encapsulation complex showed the maximum E_{ads} value. The dipole moment of the investigated complexes also experienced a significant increase in water media. In the gas phase, the Cu-doped $CuB_{11}N_{12}$-FAV complex exhibited the maximum dipole moment value at 10.16 D, followed by Cu@b66-FAV at 5.71 D, $B_{12}N_{11}Cu$-FAV at 5.65 D, Cu@b64-FAV at 5.39 D, and Cu@$B_{12}N_{12}$-FAV at 5.33 D, respectively. However, in water media, the dipole moment values increased to 14.30 D for the $CuB_{11}N_{12}$-FAV complex, 10.50 D for Cu@b64-FAV, 10.26 D for Cu@b66-FAV, 9.75 D for $B_{12}N_{11}Cu$-FAV, and 7.68 D for Cu@$B_{12}N_{12}$-FAV complex. The elevated dipole moment values in water media affirmed the ability of the investigated complexes to dissolve in polar solvents, indicating a significant increase in their reactivity, which is advantageous for FAV drug delivery applications.

As the release of drug molecules from carriers is crucial in drug delivery, evaluating the recovery time (τ) becomes significant for assessing desorption of FAV from the $B_{12}N_{12}$ nanocages. This information aids in understanding the applicability of nanocages for FAV adsorption, where high E_{ads} values correlate with longer recovery times. Sensors can be constrained by the desorption of FAV from nanocages. Examining the work of S. Thomas and M. A. Zaeem [117,118], it is clear that a brief recovery time for an adsorbent is beneficial in creating an effective sensing device. To address this aspect, we have evaluated the recovery time (τ) for drug desorption from the $B_{12}N_{12}$ nanocage surfaces is defined as Eq. (14);[119]

$$\tau = \nu_0^{-1}\exp(-E_{ads}/\kappa_b T) \quad (14)$$

Where ν_0 is the attempt frequency, k_b is Boltzmann's constant (approximately 1.99 × 10^{-3} kcal/ mol.K) [120], E_{ads} is the adsorption energy and T represents the temperature in kelvin. The recovery time for the desorption process of the FAV molecule from the Cu-doped $CuB_{11}N_{12}$-FAV complex is computed under various attempt frequencies and at three different temperatures: 298.15 K, 398.15 K, and 498.15 K, summarized in Table 7. As desorption is the inverse process of adsorption, the value of E_{ads} is assumed to be equivalent to the energy barrier (E_{activ}) for desorption. However, this assumption is unsuitable for a sensor of the FAV drug, resulting in an exceptionally low recovery time of 29.15 ns. The interaction between FAV and $CuB_{11}N_{12}$, $B_{12}N_{11}Cu$, Cu@b_{64}, Cu@$b_{66}$and Cu@$B_{12}N_{12}$ nanocages showcases strong physisorption (E_{ads} ranging from − 20.41 to −56.58 kcal mol^{-1}). Specifically, for 298.15 K (room temperature), the recovery time for the adsorption of the FAV drug molecule on the $CuB_{11}N_{12}$nanocage is calculated. This recovery time (29.01 ms), suitable for sensor applications, suggests a moderate interaction between $CuB_{11}N_{12}$ and FAV, effectively hindering the spontaneous desorption of FAV from $CuB_{11}N_{12}$ at room temperature. Thus, the Cu-modified $B_{12}N_{12}$ nanocages can act as drug delivery vehicles. Hence, the $CuB_{11}N_{12}$nanocage holds promise as a fast-response FAV sensor. Four different attempt frequencies (3.0x10^{16} HZ (ultraviolet), 7.5 × 10^{14} HZ (yellow light), 3.9x10^{14} HZ (yellow light), and 1.2x10^{14} HZ (yellow light)) were employed to comprehensively evaluate the variation in recovery time [121]. The calculated recovery times for $CuB_{11}N_{12}$ − FAV ranged from 29.15 ns to 7.25 s across different attempt frequencies and temperatures (**detailed in** Table 7). At 298.15 K and 3.0x10^{16} HZ, specifically, the recovery time of the $CuB_{11}N_{12}$ nanocage (29.01 ms) indicates potential applications, particularly as a FAV drug carrier.

Table 7
Calculated Values of Recovery Time (τ) of FAV Adsorbed $CuB_{11}N_{12}$ nanocage Using four Different Attempt Frequencies and Three Different Temperatures.

Attempt frequency	Recovery Time		
	at 298.15 K	at 398.15 K	at 498.15 K
3.0 × 10^{16} HZ(10 nm)	29.01 ms	5.13 μs	29.15 ns
7.5 × 10^{14} HZ(400 nm)	1.16 s	0.21 ms	1.17 μs
3.9 × 10^{14} HZ(760 nm)	2.23 s	0.40 ms	2.24 μs
1.2 × 10^{14} HZ(2500 nm)	7.25 s	1.28 ms	7.29 μs

We have also simulated drug adsorption and release behavior in the body conditions, $B_{12}N_{12}$-FAV and $CuB_{11}N_{12}$-FAV complexes were placed in water and an acidic environment. The conductor-like polarizable continuum model (CPCM) accounted for bulk solvent effects, with solvent energy defined as the difference between total energy in aqueous and gas phases. The pH difference between target and normal cells can trigger drug release, so the N atom of FAV drug was protonated in acidic conditions for both complexes shown in Fig. S6. DFT calculations were then performed to simulate drug release from the $B_{12}N_{12}$ and $CuB_{11}N_{12}$ nanocage complexes in an acidic environment, investigating their potential as drug delivery vehicles [122].Additionally, four water molecules were placed at the binding sites of these complexes to explicitly explore solvent effects. The interaction energies between water molecules and fullerenes were calculated using by $E_{abs(H2O-BN)} = (E_{H2O/BN} - (E_{H2O} + E_{BN}) + E_{BSSE})/4$. Table S7 lists the calculated solvent energies, water-fullerene interaction energies, and adsorption energies for $B_{12}N_{12}$-FAV and $CuB_{11}N_{12}$-FAV complexes. The interaction energies between water molecules and $B_{12}N_{12}$, as well as modified $CuB_{11}N_{12}$ nanocag, are much weaker than those between FAV drug molecules and $B_{12}N_{12}$ and modified $CuB_{11}N_{12}$ nanocages. This indicates that FAV adsorption on these nanocages is minimally affected by the surrounding water molecules. Negative adsorption energies in both aqueous and gas phases indicate favorable and spontaneous interactions between the drugs and $B_{12}N_{12}$ nanomaterials.

4. Conclusion

This study examined the efficacy of Cu-modified $B_{12}N_{12}$ nanocages ($CuB_{11}N_{12}$, $B_{12}N_{11}Cu$, Cu@b64, Cu@b66, and Cu@$B_{12}N_{12}$) as carriers for delivering the FAV drug using DFT calculations. The Cu-modified nanocages showed enhanced reactivity, higher dipole moments, and stronger interactions with the FAV drug adsorption. Negative adsorption energy values in both gas and aqueous phases indicated favorable interactions and exothermic reactions. Analysis of the most stable configurations revealed distinct structural, energetic, and electronic properties of pure $B_{12}N_{12}$ and its modified nanocages, as well as the complexes formed with FAV. Various parameters were calculated, including adsorption energy, electronic properties, dipole moment, thermodynamic parameters (ΔH and ΔG), PDOS, and relevant quantum molecular descriptors. The Cu-decorated $B_{12}N_{12}$ nanocages Cu@b64 and Cu@b66 showed significant reductions in energy gaps, from 3.28 eV and 3.33 eV to 1.54 eV and 1.59 eV, respectively, upon FAV adsorption. Thermodynamic calculations indicated that drug adsorption on these nanocages is spontaneous and exothermic. Drug adsorption in both gas and solvent phases is enhanced by doping, as confirmed by dipole moments and quantum molecular descriptors calculation. PDOS and NBO analyses revealed substantial charge transfer from the drugs to nanocages during adsorption. NCI analyses showed that drugs mainly adsorb on nanocages through weak van der Waals (vdW) interactions, facilitating effective drug release. The drug's adsorption and desorption characteristics in the solvent phase were improved by analyses of solvation effects. In low pH conditions, FAV can be separated from $B_{12}N_{12}$

and Cu-modified nanocages by H^+ proton attack, suggesting $B_{12}N_{12}$ as a promising FAV drug delivery material. In comparison to other modified nanocages, the $CuB_{11}N_{12}$ nanocage showed the shortest recovery time and proved to be more effective in drug delivery. This study provides a theoretical foundation for designing and developing $B_{12}N_{12}$ nanocages as drug carriers.

CRediT authorship contribution statement

Mohammad A. Matin: Writing – review & editing, Writing – original draft, Supervision, Formal analysis, Data curation, Conceptualization. **Joyanta K. Saha:** Writing – review & editing, Data curation, Conceptualization. **Tapas Debnath:** Writing – review & editing, Supervision, Conceptualization. **Joonkyung Jang:** Writing – review & editing, Conceptualization.

Declaration of competing interest

The authors declare that they have no known competing financial interests or personal relationships that could have appeared to influence the work reported in this paper.

Data availability

The data that has been used is confidential.

Acknowledgements

The authors sincerely thank the Computing Research Laboratory, CARS, DU, for their support in this research and gratefully acknowledge the Bangladesh Research and Education Network (BdREN) for providing the high computational power for this study. This research was supported by “Regional Innovation Strategy (RIS)” through the National Research Foundation of Korea (NRF) funded by the Ministry of Education (MOE)(2023RIS-007).

Appendix A. Supplementary data

Supplementary data to this article can be found online at https://doi.org/10.1016/j.molliq.2024.125999.

References:

[1] A.E. Allam, H.K. Assaf, H.A. Hassan, K. Shimizu, Y.A.M.M. Elshaier, RSC Adv. 10 (2020) 29983.
[2] Y. Furuta, K. Takahashi, K. Shiraki, K. Sakamoto, D.F. Smee, D.L. Barnard, B. B. Gowen, J.G. Julander, J.D. Morrey, Antiviral Res 82 (2009) 95.
[3] Y. Furuta, B.B. Gowen, K. Takahashi, K. Shiraki, D.F. Smee, D.L. Barnard, Antiviral Res 100 (2013) 446.
[4] F. Shi, Z. Li, L. Kong, Y. Xie, T. Zhang, W. Xu, Drug Discov. Ther. 8 (2014) 117.
[5] D. Butler, Nature 513 (2014) 13.
[6] S. Yamazaki, T. Suzuki, M. Sayama, T.-A. Nakada, H. Igari, I. Ishii, J. Infect. Chemother. 27 (2021) 390.
[7] M. Nasrollahzadeh, S.M. Sajadi, M. Sajjadi, Z. Issaabadi, in: Interface Science and Technology, Elsevier, 2019, pp. 1–27.
[8] S. Dongre S, S. R, C. Hunsur Ravikumar, L. C, R.G. Balakrishna, Adv. Mater. Interfaces 9 (2022) 2200442.
[9] Z.-Q. Feng, K. Yan, J. Li, X. Xu, T. Yuan, T. Wang, J. Zheng, Mater. Sci. Eng. C 104 (2019) 110001.
[10] H. Khalafi, S. Ahmadi, Z.M. Kotena, J. Mol. Struct. 1247 (2022) 131360.
[11] A. Soltani, M. Ramezanitaghartapeh, M.B. Javan, M.T. Baei, A.N.K. Lup, P. J. Mahon, M. Aghaei, New J. Chem. 44 (2020) 14513.
[12] S. Ding, W. Gu, J. Mol. Liq. 345 (2022) 117041.
[13] J. Zhao, Q. Du, S. Zhou, V. Kumar, Chem Rev 120 (2020) 9021.
[14] S. Patel, P. Patel, D. Chodvadiya, N.N. Som, P.K. Jha, J. Mol. Liq. 352 (2022) 118702.
[15] M. Shamima Khanom, M. Rakib Hossain, K. Zahirul Islam, M. Abul Hossain, F. Ahmed, Comput. Theor. Chem. 1216 (2022) 113869.
[16] F. Rahimi, A. Zabaradsti, J. Inorg. Orgonat. Polym. Mater. 27 (2017) 1770.
[17] S. Hussain, R. Hussain, M.Y. Mehboob, S.A.S. Chatha, A.I. Hussain, A. Umar, M. U. Khan, M. Ahmed, M. Adnan, K. Ayub, ACS Omega 5 (2020) 7641.
[18] H.Y. Ammar, H.M. Badran, K.M. Eid, Mater. Today Commun. 25 (2020) 101681.
[19] A. Escobedo-Morales, M. Salazar-Villanueva, H. Guatemala-Vera, M.S. Pedraza-Chan, J.H. Camacho-García, E. Chigo-Anota, Adv. Theor. Simul. 7 (2024) 2300698.
[20] F. Jensen, H. Toftlund, Chem. Phys. Lett. 201 (1993) 89.
[21] D.L. Strout, J. Phys. Chem. A 104 (2000) 3364.
[22] W. Xie, J. Wang, J. Wang, X. Wu, Z. Wang, R.-Q. Zhang, J. Phys. Chem. C 124 (2020) 3881.
[23] G. Seifert, P.W. Fowler, D. Mitchell, D. Porezag, T. Frauenheim, Chem. Phys. Lett. 268 (1997) 352.
[24] T. Oku, A. Nishiwaki, I. Narita, Sci. Technol. Adv. Mater. 5 (2004) 635.
[25] Y.-C. Zhu, Y. Bando, L.-W. Yin, D. Golberg, Chem. Eur. J. 10 (2004) 3667.
[26] T. Oku, A. Nishiwaki, I. Narita, Solid State Commun. 130 (2004) 171.
[27] T. Oku, Energies 8 (2015) 319.
[28] M. Kurban, İ. Muz, Struct. Chem. 34 (2023) 1061.
[29] İ. Muz, S. Alaei, M. Kurban, Mater. Today Commun. 27 (2021) 102252.
[30] İ. Muz, F. Göktaş, M. Kurban, Chem. Phys. 539 (2020) 110929.
[31] S. Lin, X. Wang, Y. Yang, X. Meng, Y. Qu, Y.-Q. Li, M. Zhao, X. Liu, W. Li, J. Phys. D: Appl. Phys. 55 (2022) 295401.
[32] K.D. Patel, R.K. Singh, H.-W. Kim, Mater. Horiz. 6 (2019) 434.
[33] A. Merlo, V.R.S.S. Mokkapati, S. Pandit, I. Mijakovic, Biomater. Sci. 6 (2018) 2298.
[34] K.A. Soliman, S.A. Aal, Diam. Relat. Mater. 117 (2021) 108458.
[35] Y. Cao, A. Khan, H. Balakheyli, A.N.K. Lup, M. Ramezani Taghartapeh, H. Mirzaei, S. Reza Khandoozi, A. Soltani, M. Aghaei, F. Heidari, S.M. Sarkar, A.B. Albadarin, Arab. J. Chem. 14 (2021) 103200.
[36] M.K. Hazrati, N.L. Hadipour, Phys. Lett. A 380 (2016) 937.
[37] A. Soltani, A. Sousaraei, M. Bezi Javan, M. Eskandari, H. Balakheyli, New J. Chem. 40 (2016) 7018.
[38] D.V. Shtansky, K.L. Firestein, D.V. Golberg, Nanoscale 10 (2018) 17477.
[39] C. Parlak, Ö. Alver, M. Şenyel, J. Theor. Comput. Chem. 16 (2017) 1750011.
[40] A.S. Rad, M. Ardjmand, M.R. Esfahani, B. Khodashenas, Spectrochim. Acta Part A: Mol. Biomol. Spectrosc. 247 (2021) 119082.
[41] R. Guo, Q. Liu, W. Wang, R. Tayebee, F. Mollania, J. Mol. Liq. 325 (2021) 114798.
[42] K. Chukwuemeka, H. Louis, I. Benjamin, P.A. Nyong, E.U. Ejiofor, E.A. Eno, A.-L.-E. Manicum, ACS Appl. Bio Mater. 6 (2023) 1146.
[43] M. Kurban, İ. Muz, J. Mol. Liq. 309 (2020) 113209.
[44] E. Shakerzadeh, K.K. Zborowski, E.C. Anota, M.T. Nguyen, Appl. Organometl. Chem. 36 (2022) e6721.
[45] N. Abdolahi, P. Singla, A. Soltani, M. Javan, M. Aghaei, F. Heidari, S. Sedighi, Physica e: Low-Dimensional Syst. Nanostruct. 124 (2020) 114296.
[46] Y. Cao, A. Khan, F. Ghorbani, H. Mirzaei, P. Singla, H. Balakheyli, A. Soltani, M. Aghaei, Z. Azmoodeh, M. Aarabi, S. Tavassoli, J. Mol. Liq. 339 (2021) 116678.
[47] A. Soltani, M.R. Taghartapeh, V. Erfani-Moghadam, M.B. Javan, F. Heidari, M. Aghaei, P.J. Mahon, Mater. Sci. Eng. C 92 (2018) 216.
[48] İ. Muz, Mater. Today Commun. 31 (2022) 103798.
[49] Y. Lai, T.J. Al-Musawi, U. Abdul-Reda Hussein, I. Waleed, H. Hassan Ahmed, A. Qasim Khallawi, K. Majid Alsaraf, M. Asiri, M. Abosaooda, H.O. Alsaab, J. Mol. Liq. 384 (2023) 122260.
[50] M.R. Hossain, M.M. Hasan, M. Nishat, E.A. Noor, F. Ahmed, T. Ferdous, M. A. Hossain, J. Mol. Liq. 323 (2021) 114627.
[51] H.R.A. El-Mageed, M.A.A. Ibrahim, J. Mol. Liq. 326 (2021) 115297.
[52] X. Yao, J. Mu, Y. Zheng, J. Wu, W. Zhu, K. Wang, Colloids Surface A 678 (2023) 132481.
[53] S.U.D. Shamim, M.H. Miah, M.R. Hossain, M.M. Hasan, M.K. Hossain, M. A. Hossain, F. Ahmed, Physica e: Low-Dimensional Syst. Nanostruct. 136 (2022) 115027.
[54] P. Dhali, A.K.M.A. Hossain, J. Mol. Liq. 396 (2024) 124051.
[55] G. Mehraein, M. Rezaei-Sameti, E. Asgary, M. Aghamohammadi, J. Mol. Struct. 1248 (2022) 131478.
[56] Y. Cao, A. Khan, H. Mirzaei, S. Reza Khandoozi, M. Javan, A. Ng Kay Lup, A. Norouzi, E. Tazikeh Lemeski, M. Pishnamazi, A. Soltani, A.B. Albadarin, J. Mol. Liq. 334 (2021) 116516.
[57] M. Suliman, M. Hadi Kzar, A.S.M. Juma, I. Abbas Ali, Y. Yasin, N. Hassan Sayyid, A. Taan Alkhafaji, A.J. Kadhim, M.M. Abid, A. Hussien Alawadi, A. Alsalamy, J. Kaur, E. Tazikeh-Lemeski, S. Moazen Rad, A. Soltani, J. Mol. Liq. 395 (2024) 123816.
[58] M. Khaleghian, M. Sheikhi, S. Shahab, S. Kaviani, Comput. Theor. Chem. 1237 (2024) 114616.
[59] M.M. Hasan, A.C. Das, M.R. Hossain, M.K. Hossain, M.A. Hossain, B. Neher, F. Ahmed, J. Biomolecular Struct. Dyn. 40 (2022) 13190.
[60] İ. Muz, F. Göktaş, M. Kurban, Physica e: Low-Dimensional Syst. Nanostruct. 135 (2022) 114950.
[61] M.A. Matin, M. Alauddin, M.M. Islam, J. Mol. Liq. 407 (2024) 125244.
[62] M. Kurban, İ. Muz, Mater. Today Commun. 38 (2024) 108488.
[63] R. Gholami, M. Solimannejad, J. Mol. Struct. 1270 (2022) 133968.
[64] F. Pan, A.T. Jalil, F. Alsaikhan, M. Adil, A.J. Kadhim, D.A.A.-a. Amran, M. Abosaooda, A.S. Altamimi, S.M.D. Younis, A.N.K. Lup, S. Tavassoli, H. Balakheyli, A. Soltani, Diam. Relat. Mater. 136 (2023) 110044.
[65] E. Hosseinzadeh, A. Foroumadi, L. Firoozpour, J. Mol. Liq. 374 (2023) 121262.
[66] S. Kaviani, S. Shahab, M. Sheikhi, Physica e: Low-Dimens. Syst. Nanostruct. 126 (2021) 114473.
[67] M.H. Miah, M.R. Hossain, M.S. Islam, T. Ferdous, F. Ahmed, RSC Adv. 11 (2021) 38457.
[68] Z. Liao, G. Song, Z. Yang, H. Ren, Mol. Phys. 119 (2021) e1921296.
[69] İ. Muz, M. Kurban, J. Mol. Liq. 335 (2021) 116181.

[70] A. Gholami, E. Shakerzadeh, E. Chigo Anota, M. corazon Flores Bautista, Inorg. Chem. Commun. 148 (2023) 110326.
[71] A.A. Piya, A.K.M.A. Hossain, RSC Adv. 13 (2023) 27309.
[72] Z.M. Shabavi, E. Shakerzadeh, T. Yadav, E. Tahmasebi, S. Kaviani, E.C. Anota, Comput. Theor. Chem. 1234 (2024) 114535.
[73] Z.M. Shabavi, E. Shakerzadeh, T. Yadav, E.C. Anota, Diam. Relat. Mater. 148 (2024) 111463.
[74] H.O. Edet, H. Louis, T.E. Gber, P.S. Idante, T.C. Egemonye, P.B. Ashishie, E. E. Oyo-Ita, I. Benjamin, A.S. Adeyinka, Heliyon 9 (2023) e12599.
[75] M. Sadat Mussavi, S. Hosseini, J. Mol. Liq. 395 (2024) 123900.
[76] M.A.A. Ibrahim, A.-S.-S.-M. Rady, P.A. Sidhom, S.R.M. Sayed, K.E. Ibrahim, A. M. Awad, T. Shoeib, L.A. Mohamed, ACS Omega 9 (2024) 25203.
[77] A. Maleki, Struct. Chem. 33 (2022) 323.
[78] A.U. Rahman, D.M. Saaduzzaman, S.M. Hasan, M.K.U. Sikder, New J. Chem (2024).
[79] M. Pishnamazi, S.M. Alshahrani, H. Faris Alotaibi, J. Mol. Liq. 410 (2024) 125541.
[80] A. Maleki, S. Esmaielzadeh, S. Fakhraee, Theor Chem Acc. 143 (2024) 39.
[81] S. Ketabi, S. Shalmashi, S. Hallajian, BMC Chemistry 17 (2023) 169.
[82] A.J. Bin Iqbal, R. Shahriar, A. Zubair, Nanoscale Adv. 6 (2024) 2968.
[83] Y. Zhang, Y. Luo, L. Tang, M. E, J. Hu, J. Mol. Liq. 393 (2024) 123607.
[84] H.A. Rizwan, M.U. Khan, A. Anwar, M.U. Khan, A. Sohail, S. Ahmed, S. M. Alshehri, Surf. Interfaces 51 (2024) 104779.
[85] A.L. Pereira Silva, J.J.G. Varela Júnior, Inorg. Chem. 62 (2023) 1926.
[86] M.J. Frisch, G.W. Trucks, H.B. Schlegel, G.E. Scuseria, M.A. Robb, J.R. Cheeseman, G. Scalmani, V. Barone, G.A. Petersson, H. Nakatsuji, X. Li, M. Caricato, A.V. Marenich, J. Bloino, B.G. Janesko, R. Gomperts, B. Mennucci, H.P. Hratchian, J.V. Ortiz, A.F. Izmaylov, J.L. Sonnenberg, Williams, F. Ding, F. Lipparini, F. Egidi, J. Goings, B. Peng, A. Petrone, T. Henderson, D. Ranasinghe, V.G. Zakrzewski, J. Gao, N. Rega, G. Zheng, W. Liang, M. Hada, M. Ehara, K. Toyota, R. Fukuda, J. Hasegawa, M. Ishida, T. Nakajima, Y. Honda, O. Kitao, H. Nakai, T. Vreven, K. Throssell, J.A. Montgomery Jr., J.E. Peralta, F. Ogliaro, M.J. Bearpark, J.J. Heyd, E.N. Brothers, K.N. Kudin, V.N. Staroverov, T.A. Keith, R. Kobayashi, J. Normand, K. Raghavachari, A.P. Rendell, J.C. Burant, S.S. Iyengar, J. Tomasi, M. Cossi, J.M. Millam, M. Klene, C. Adamo, R. Cammi, J.W. Ochterski, R.L. Martin, K. Morokuma, O. Farkas, J.B. Foresman, D.J. Fox, Wallingford, CT, 2016.
[87] S. Wu, L. Li, Q. Liang, H. Gao, T. Tang, Y. Tang, New J. Chem. 47 (2023) 21743.
[88] A. el-Krim Sandeli, N. Khiri-Meribout, S. Benzerka, H. Boulebd, N. Gürbüz, N. Özdemir, İ. Özdemir, New J. Chem. 45 (2021) 17878.
[89] M.R.S.A. Janjua, Inorg. Chem. 60 (2021) 10837.
[90] S.F. Boys, F. Bernardi, Mol. Phys. 19 (1970) 553.
[91] J. Tomasi, B. Mennucci, R. Cammi, Chem. Rev. 105 (2005) 2999.
[92] M. Cossi, V. Barone, R. Cammi, J. Tomasi, Chem. Phys. Lett. 255 (1996) 327.
[93] N.M. O'boyle, A.L. Tenderholt, K.M. Langner, J. Comput. Chem. 29 (2008) 839.
[94] W. Humphrey, A. Dalke, K. Schulten, J. Mol. Graph. 14 (1996) 33.
[95] T. Lu, F. Chen, J. Comput. Chem. 33 (2012) 580.
[96] S. Bibi, S. Ur-rehman, L. Khalid, I.A. Bhatti, H.N. Bhatti, J. Iqbal, F.Q. Bai, H.-X. Zhang, RSC Adv. 12 (2022) 2873.
[97] T. Sutradhar, A. Misra, J. Phys. Chem. A 125 (2021) 2436.
[98] S. Larki, E. Shakerzadeh, E.C. Anota, R. Behjatmanesh-Ardakani, Chem. Phys. 526 (2019) 110424.
[99] M.D. Esrafili, H. Abdollahpour, N. Saeidi, Chem. Select 3 (2018) 1168.
[100] Z. Zhao, Z. Li, Q. Wang, Chem. Phys. Lett. 739 (2020) 136922.
[101] A. Soltani, E. Tazikeh-Lemeski, M.B. Javan, J. Mol. Liq. 297 (2020) 111894.
[102] A.L.P. Silva, A.C.A. Silva, J.d.J.G. Varela Júnior, Comput. Theor. Chem. (2022, 1215,) 113836.
[103] L. Zhang, X. Cheng, X.-H. Li, J.-H. Chen, W.-M. Sun, J. Mol. Liq. 360 (2022) 119388.
[104] S. Thomas, M. Asle Zaeem, Appl. Surf. Sci. 563 (2021) 150232.
[105] T. Kaewmaraya, L. Ngamwongwan, P. Moontragoon, A. Karton, T. Hussain, J. Phys. Chem. C 122 (2018) 20186.
[106] N. Wazzan, K.A. Soliman, W.S.A. Halim, J. Mol. Model. 25 (2019) 265.
[107] M. Rakib Hossain, M. Mehade Hasan, S. Ud Daula Shamim, T. Ferdous, M. Abul Hossain, F. Ahmed, Comput. Theor. Chem. 1197 (2021) 113156.
[108] T. Kaewmaraya, L. Ngamwongwan, P. Moontragoon, W. Jarernboon, D. Singh, R. Ahuja, A. Karton, T. Hussain, J. Hazard. Mater. 401 (2021) 123340.
[109] İ. Muz, F. Göktaş, M. Kurban, Theor. Chem. Acc. 139 (2020) 23.
[110] S.S. Li, in: Semiconductor Physical Electronics, Springer, New York, New York, NY, 2006, pp. 211–245.
[111] F. Mollania, N.L. Hadipour, N. Mollania, J. Biotech. 308 (2020) 40.
[112] E. Mirhaji, M. Afshar, S. Rezvani, M. Yoosefian, J. Mol. Liq. 271 (2018) 151.
[113] J.P. Cachaneski-Lopes, A. Batagin-Neto, J. Nanostruc. Chem. 12 (2022) 141.
[114] S. Dushman, Rev. Modern Phys. 2 (1930) 381.
[115] E.R. Johnson, S. Keinan, P. Mori-Sánchez, J. Contreras-García, A.J. Cohen, W. Yang, J. Am. Chem. Soc. 132 (2010) 6498.
[116] J.K. Saha, J. Raihan, M.A. Matin, J. Jang, Struc. Chem. 35 (2024) 297.
[117] S. Thomas, M. Asle Zaeem, Adv. Theory Simul. 4 (2021) 2000250.
[118] S. Thomas, V. Kumar, D.R. Roy, M.A. Zaeem, A.C.S. Appl, Nano Mater. 3 (2020) 10073.
[119] H.O. Muhsen, A.O.M. Almayyali, A.Y. Al-Mamoori, F.F. Mahmood, J. Mol Model 27 (2021) 90.
[120] M.A.A. Ibrahim, A.-s.S.M. Rady, L.A. Mohamed, A.M. Shawky, T.H.A. Hasanin, P. A. Sidhom, N.A.M. Moussa, J. Biomol. Struct. Dyn. 41 (2023) 12923.
[121] D. Paul, A. Vaidyanathan, U. Sarkar, B. Chakraborty, Struc. Chem. 32 (2021).
[122] M. Kanamala, W.R. Wilson, M. Yang, B.D. Palmer, Z. Wu, Biomaterials 85 (2016) 152.